

## Article

# Projection of Future Climate Change and Its Influence on Surface Runoff of the Upper Yangtze River Basin, China

Hanli Wan

Key Laboratory of Mountain Surface Processes and Ecological Regulation, Institute of Mountain Hazards and Environment, Chinese Academy of Sciences, Chengdu 610041, China; wanhanli@imde.ac.cn

**Abstract:** Global climate change will modify precipitation and temperatures' temporal and spatial distribution, trigger more extreme weather events, and impact hydrological processes. The Yangtze River basin is one of the world's largest basins, and understanding future climate changes is vital for water resource management and supply. Research on predicting future climate change in the upper Yangtze River basin (UYRB) and introducing machine learning algorithms to analyze the impact of climate factors, including extreme weather indicators, on surface runoff is urgently needed. In this study, a statistical downscaling model (SDSM) was used to forecast the future climate in the UYRB, and the Mann–Kendall (MK) or modified Mann–Kendall (MMK) trend test at a 5% level of significance was applied to analyze temporal trends. The Spearman rank correlation (SRC) test at a 5% level of significance and random forest regression (RFR) model were employed to identify the key climatic factors affecting surface runoff from annual precipitation, annual temperature, maximum 5-day precipitation ( $R \times 5\text{Day}$ ), number of tropical nights (TR), and consecutive dry days (CDD), and the RFR model was also used to predict future runoff. Based on the results, we found that, compared to the selected historical period (1985–2014), the mean annual precipitation (temperature) during the mid-term (2036–2065) increased by 18.93% (12.77%), 17.78% (14.68%), 20.03% (17.03%), and 19.67% (19.29%) under SSP1-2.6, SSP2-4.5, SSP3-7.0, and SSP5-8.5, respectively, and during the long term (2071–2100), increased by 19.44% (12.95%), 22.01% (21.37%), 30.31% (30.32%), and 34.48% (37.97%), respectively. The warming and humidification characteristics of the northwestern UYRB were more pronounced. The key climatic factors influencing surface runoff were annual precipitation, maximum 5-day precipitation ( $R \times 5\text{day}$ ), and annual temperature. Because of warming and humidification, surface runoff in the UYRB is expected to increase relative to the historical period. The surface runoff during the mid-term (long term) increased by 12.09% (12.58%), 8.15% (6.84%), 8.86% (8.87%), and 5.77% (6.21%) under SSP1-2.6, SSP2-4.5, SSP3-7.0, and SSP5-8.5, respectively. The implementation of sustainable development pathways under the low radiative forcing scenario can be effective in mitigating climate change, but at the same time, it may increase the risk of floods in the UYRB.

**Keywords:** climate change; hydroclimatic variables; runoff; the upper Yangtze River basin; spatio-temporal variability



**Citation:** Wan, H. Projection of Future Climate Change and Its Influence on Surface Runoff of the Upper Yangtze River Basin, China. *Atmosphere* **2023**, *14*, 1576. <https://doi.org/10.3390/atmos14101576>

Received: 31 July 2023

Revised: 30 September 2023

Accepted: 6 October 2023

Published: 18 October 2023



**Copyright:** © 2023 by the author. Licensee MDPI, Basel, Switzerland. This article is an open access article distributed under the terms and conditions of the Creative Commons Attribution (CC BY) license (<https://creativecommons.org/licenses/by/4.0/>).

## 1. Introduction

Global climate change has become a significant challenge facing humanity and has received extensive attention from society and academia [1,2]. The sixth assessment report of the Intergovernmental Panel on Climate Change (IPCC) pointed out that climate change has caused tremendous damage and increasingly irreversible losses to terrestrial, freshwater, coastal, and marine ecosystems [3–10]. As climatic conditions are closely related to the hydrological cycle, it is important to study climate change for regional and global water resource management and utilization [11–14].

Temperature and precipitation are the basic meteorological factors [15]. Climate change has changed the spatial and temporal distribution patterns of global temperature and precipitation and increased the probability of extreme weather events in more than 80%

of the world [16]. Climate change exhibits global and regional characteristics influenced by various factors. Different regions have distinct climate change features. In areas with complex topographies and volatile local climates, the regional natural conditions are more sensitive to climate change, making the resulting impacts worthy of further research.

Climate change affects the hydrological cycle [17,18]. Global warming is accelerating the hydrological cycle and changing the intensity and frequency of precipitation. Moreover, precipitation is directly involved in the hydrological cycle, changing the runoff of the basin [16,19,20]. The increase in temperature has changed the water resources' temporal and spatial distribution and increased the probability of extreme climate events [21,22].

Studies on rainfall–runoff modeling show that precipitation is an important recharge source for surface runoff, and regional surface runoff is highly sensitive to changes in precipitation [23–25]. The increase in temperature leads to an increase in the evaporation of soil moisture and surface runoff and a decrease in streamflow [26–28]. Climate change has enhanced the temporal and spatial variability of precipitation and temperature, leading to the frequent occurrence of extreme weather events. Extreme weather events such as hot extreme rainstorms are more likely to cause drought and flood disasters [29], which greatly reduce the utilization capacity of regional water resources and cause significant damage to the ecological environment and human social economy [11,16,30].

Extreme climatic factors need more attention in studies on surface runoff and climate. Existing studies are usually conducted at the administrative scale, and few studies have been conducted at the large watershed scale where climatic conditions are complex [31,32]. In addition, most studies have utilized statistical methods, such as linear regression, multiple linear regression, or nonparametric tests, to identify correlations between climatic factors and surface runoff and to identify factors that influence surface runoff [27,33–35]. However, these methods make it difficult to accurately capture the relationship between climatic factors and surface runoff. This results in low confidence in the identification of key factors affecting surface runoff.

Machine learning is a technique that utilizes algorithms to learn from data and automatically improve the performance of a system. In machine learning, algorithms learn laws and patterns from input data and make predictions or decisions about new data based on these laws and patterns [36]. Machine learning techniques can be categorized into three types: supervised learning, unsupervised learning, and reinforcement learning. With the enhancement of the computing power of devices and the increase in data volume, machine-learning algorithms have been widely applied in the field of hydrometeorology, including the establishment of prediction models, decision-making classifications, and data mining [37–42]. In the study of capturing the correlation between surface runoff and climatic factors and deciding the key factors affecting surface runoff, the application of machine-learning algorithms is expected to enhance the credibility of the conclusions.

The Yangtze River, the longest river in Asia and the third longest in the world, spans 6300 km [8,43]. The upper Yangtze River basin (UYRB) is characterized by complex terrain and is significantly influenced by the Qinghai–Tibet Plateau, southwest monsoon, and southeast monsoon. The region is sensitive and vulnerable to climate change [44]. Against the backdrop of global warming, the frequency and intensity of droughts and floods in the upstream Yangtze River region have increased. Aquatic and terrestrial ecosystems are deteriorating, leading to frequent natural disasters. These factors severely impede the sustainable socioeconomic development of the Yangtze River basin [45]. In the future, climate change will likely alter the hydrological cycle and runoff processes in the UYRB. This has a more pronounced impact on the distribution of water resources in the UYRB. It also adversely affects the water resources for hydropower generation and agricultural irrigation.

At present, research on predicting future climate change in the UYRB and introducing machine learning algorithms to analyze the impact of climate factors, including extreme weather indicators, on surface runoff is urgently needed. To achieve these goals, this study utilized meteorological observation data from 1985 to 2014 in the UYRB and general circulation model (GCM) data under shared socioeconomic pathways (SSP) scenarios. A

statistical downscaling model, a random forest regression model, and a multiple regression model were employed to predict future precipitation, temperature, and runoff in the UYRB. The specific research objectives were as follows: (1) to analyze the spatiotemporal precipitation and temperature patterns in the UYRB; (2) to forecast spatiotemporal changes in precipitation and temperature in the UYRB under different SSP scenarios; (3) to identify the key climatic factors influencing runoff in the UYRB and predict trends of surface runoff changes.

## 2. Materials and Methods

### 2.1. Research Area

The Yangtze River originates in the Tanggula Mountains in the Qinghai–Tibet Plateau, with a total length of 6300 km. Yichang, Hubei Province, serves as the dividing point between the upper and lower reaches of the Yangtze River. The upper Yangtze River basin (UYRB) is located between  $90^{\circ}32' \sim 111^{\circ}33'$  E and  $24^{\circ}42' \sim 35^{\circ}55'$  N (Figure 1). It spans approximately 4500 km in length and covers an area of  $100 \text{ km}^2$ , which accounts for over half of the total Yangtze River basin area. The UYRB encompasses nine provinces, municipalities, and autonomous regions, including Yunnan, Sichuan, and Guizhou [11,30]. The topography of the UYRB is characterized by significant variations, with the land elevation gradually decreasing from west to east. The regional elevation difference can reach up to 7000 m. The river flows through the Qinghai–Tibet Plateau, Yungui Plateau, eastern extension of the Qinling Mountains, and Sichuan basin. The terrain and landforms within the UYRB are diverse and complex, with the largest areas occupied by mountains and plateaus, accounting for 50% and 30% of the total area of the UYRB, respectively. Hills account for 18% of the area, while plains make up only 2% [46].

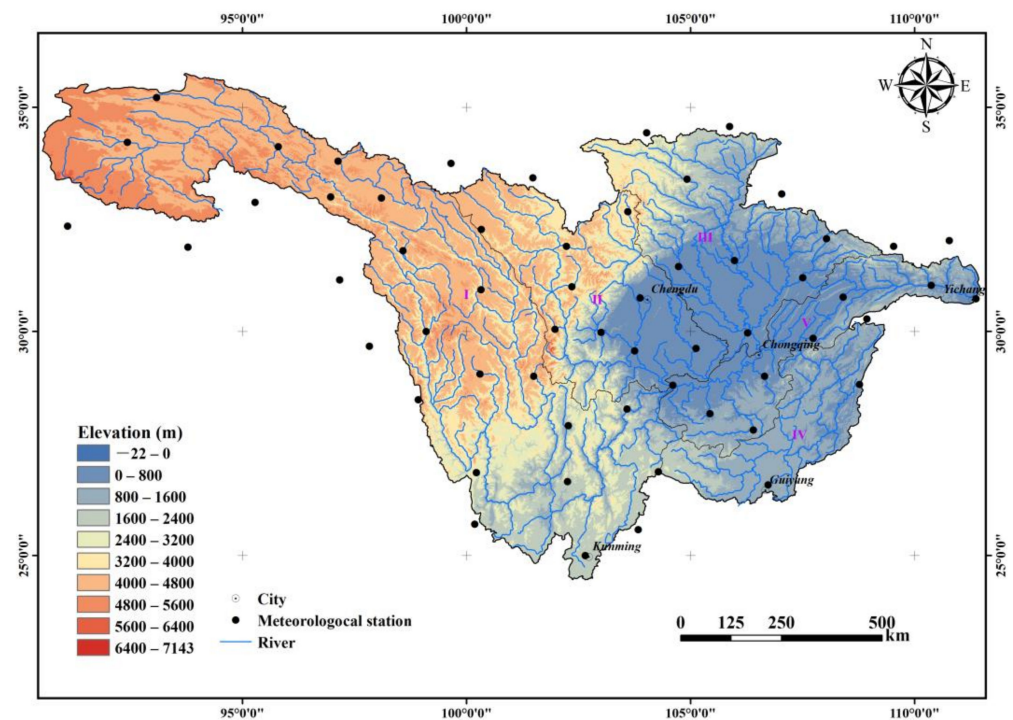


**Figure 1.** Location of the upper Yangtze River basin, meteorological stations, and the five sub-basins. (I) Jinsha River basin; (II) Mintuo River basin; (III) Jialing River basin; (IV) Wu River basin; (V) Yibin–Yichang River basin.

The climate in the UYRB exhibits distinctive patterns on both temporal and spatial scales due to the influences of the East Asian monsoon, the South Asian monsoon, and the topography of the Qinghai–Tibet Plateau. At the temporal scale, the climate in the UYRB exhibits significant interannual variations, uneven seasonal distribution, and notable

rainy and hot periods. The annual precipitation over multiple years in the UYRB ranges from 723 to 1134 mm, with an annual temperature of 8.6 to 16.8 °C. Precipitation in the basin is concentrated from April to October (Figure 2a), accounting for over 90% of the total annual precipitation. Moreover, the monthly average temperatures during this period remain above 10 °C. Throughout the year, the precipitation (temperature) in the UYRB gradually increases from January, reaches its peak in July at 162.81 mm (20.31 °C), and then gradually decreases.

At the spatial scale, the climate conditions in the UYRB also exhibit considerable variability. Specifically, the western high-altitude areas have a cold, temperate climate characterized by long winters. The majority of the remaining areas, with elevations below 3000 m, are influenced by the East Asian monsoon and the West Asian monsoon, resulting in abundant rainfall and considerable heat. Annual precipitation can reflect the moisture level of a region. Typically, areas with annual precipitation above 800 mm are classified as “humid regions”, while areas with precipitation between 400 and 800 mm fall into the category of “semi-humid regions.” Areas with precipitation ranging from 200 to 400 mm are classified as “semi-arid regions”, and areas with precipitation below 200 mm are categorized as “arid regions.” As shown in Figure 2b, the mean annual precipitation in the UYRB increases from northwest to southeast and is sequentially distributed in semi-arid, semi-humid, and humid regions. The area of humid regions accounts for about 50% of the total area of the UYRB, mainly distributed in the Wu River basin, Yibin–Yichang River basin, and downstream of the other three sub-basins. Figure 2c illustrates that the mean annual average temperature also increases from northwest to southeast. Cold regions with mean annual temperatures below 0 °C are concentrated in the high-altitude areas in the northwest, with elevations exceeding 4000 m. The mean annual temperature in the central and eastern parts of the UYRB ranges from 14 to 20 °C.

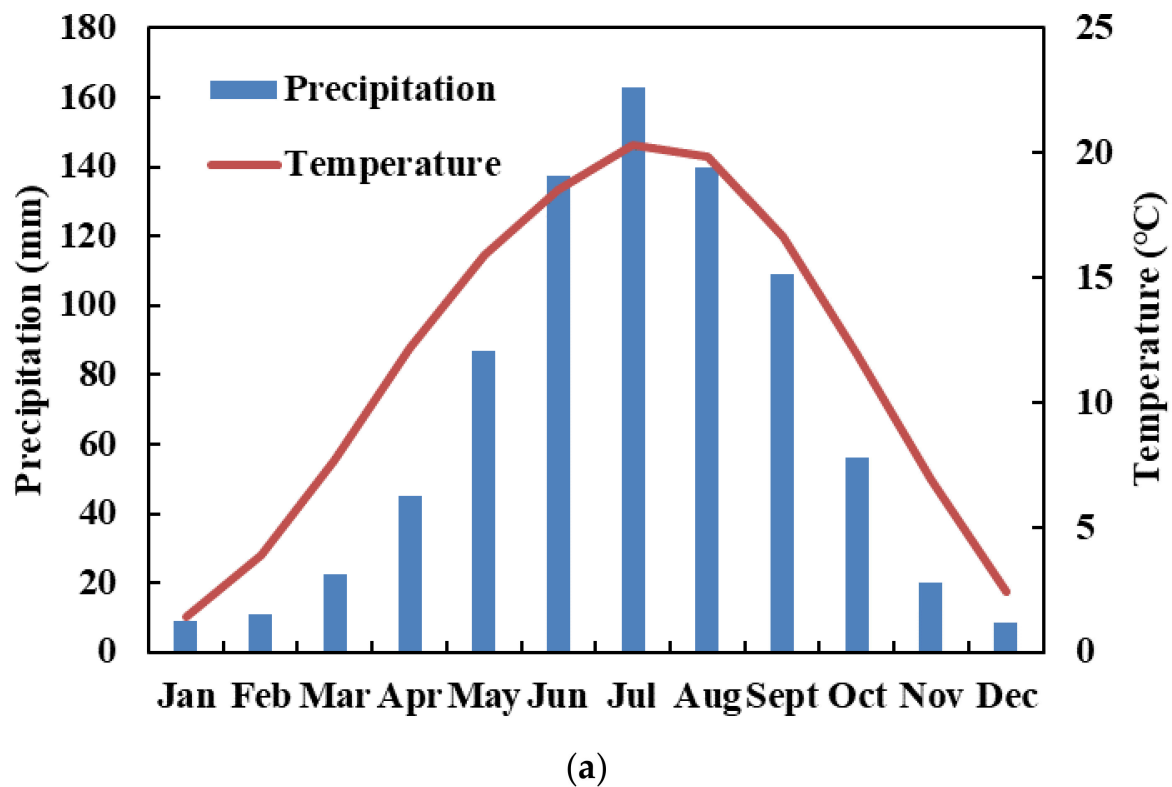
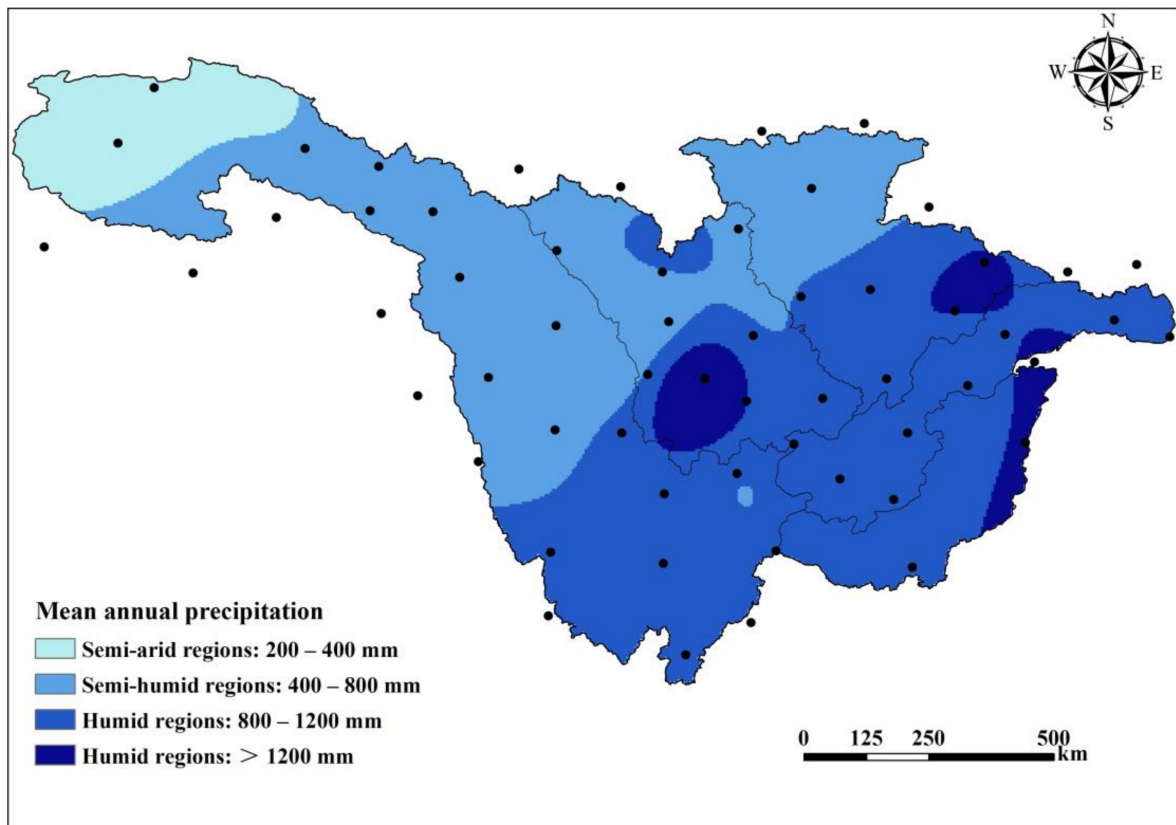
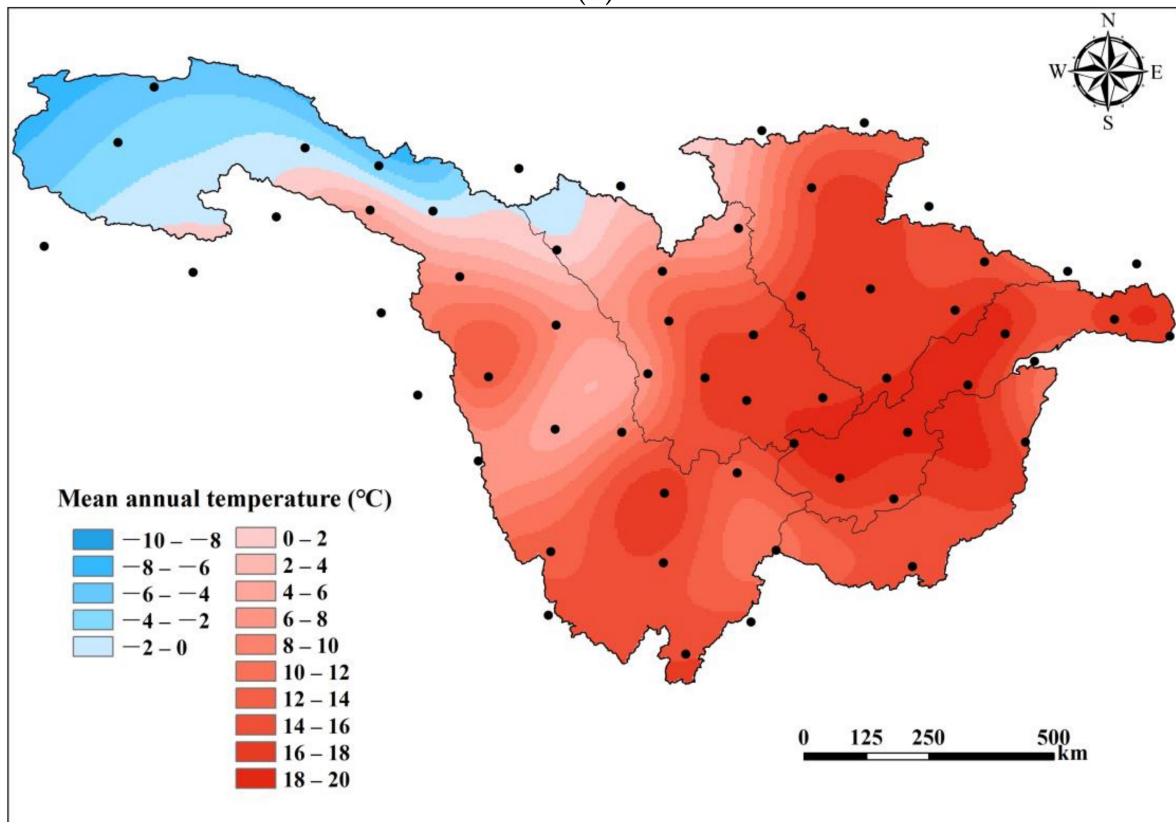


Figure 2. Cont.



(b)



(c)

**Figure 2.** The temporal and spatial patterns of climate in the UYRB (1985–2014), (a) monthly precipitation and temperature, (b) mean annual precipitation, (c) mean annual average temperature.

## 2.2. Data

The observed precipitation, temperature data, and NCEP-DOE Reanalysis 2 (R-2) dataset were employed in this study to establish a statistical downscaling model for the UYRB. The CMIP6 climate data was utilized for predicting future climate. A comprehensive description of the data is provided below:

The daily precipitation and temperature data were sourced from the National Meteorological Science Data Center (<http://data.cma.cn/>, accessed on 15 June 2023). A total of 58 meteorological stations within and around the UYRB were included, as depicted in Figure 1. The information for all stations can be found in Table A1. The observed data covers the period from 1985 to 2014 (1999–2014 for Dongxing station). Missing values were represented by −999, enabling proper identification of data sequences when applying the statistical downscaling model (SDSM).

The annual surface runoff records of Yichang hydrologic station, the outlet of the UYRB, were collected from the literature [8]. Surface runoff data covers the period of 1985–2014. The surface runoff data were converted into surface runoff depth (mm) for subsequent analysis.

NCEP-DOE Reanalysis 2 (R-2) was utilized for constructing the SDSM as the input dataset [47]. It should be noted that the dataset used is an improved version of its predecessor, NCEP/NCAR Reanalysis 1, as it includes updated parameterizations of physical processes and error fixes [47]. NCEP-DOE Reanalysis 2 (R-2) dataset covers the same time period as the observed data, which is from 1985 to 2014.

The CMIP6 daily predictor variables from the Canadian Earth System Model version 5 (CanESM5), the Max Planck Institute for Meteorology Earth System Model version 1.2 (MPI-ESM1.2), and the Norwegian Earth System Model version 2 (NorESM2) experiments were used to project climate change in the UYRB over a medium future period (2036–2065) and long-term future period (2071–2100). Four SSP datasets were used, including SSP1-2.6, SSP2-4.5, SSP3-7.0, and SSP5-8.5. The R-2 and CMIP6 daily predictors are all grid datasets. The grid has a uniform longitudinal/latitudinal resolution of 2.8125° [47].

All predictor variables were standardized. The 1985–2014 date range was selected as the reference period for standardization of the predictor variables [48,49]. Standardized values ( $n$ ) are produced from predictor values ( $x$ ) utilizing the mean ( $\mu$ ) and standard deviation ( $\sigma$ ) over the 1985–2014 reference period for each data source and according to individual grid boxes using the following expression:

$$n_i = \frac{(x_i - \mu_{1985-2014})}{\sigma_{1985-2014}} \quad (1)$$

## 2.3. Methods

To carry out the purpose of this paper, the following methods were used: (1) Statistical downscaling model (SDSM) was employed to project future precipitation and temperature in UYRB; (2) Mann–Kendall (MK)/modified Mann–Kendall (MMK) trend test and Theil–Sen’s slope were utilized to assess the trends and the trend magnitudes; (3) extreme weather indicators recommended by ECTTDI, such as number of tropical nights (TR), maximum consecutive 5-day precipitation ( $R \times 5\text{day}$ ), and consecutive dry days (CDD), were used to measure extreme climate events. The definitions of extreme climate indices can be seen in Table 1 [43,44]; (4) the Spearman rank correlation test (SRC) and random forest regression (RFR) model were employed to identify the key climatic factors that influence runoff; (5) multiple regression model was applied to predicting runoff; (6) some other common statistical analysis methods were used in this research.

**Table 1.** Definitions of extreme weather indicators [43,44].

Indicators	Name	Definition	Units
TR	Number of tropical nights	Number of days on which daily minimum temperature > 20 °C	days
R×5day	Maximum 5-day precipitation	Annual maximum consecutive 5-day precipitation	mm
CDD	Consecutive dry days	Maximum number of consecutive dry days (when daily precipitation <1.0 mm)	days

2.3.1. Statistical Downscaling Model

The general circulation model (GCM) is currently the most feasible method for large-scale climate simulation and climate change prediction research. However, the characteristics of GCM data are large-scale and low-resolution, which makes GCM data unable to meet the needs of regional studies for high-resolution meteorological data [50]. The downscaling methods of large-scale climate data usually include statistical downscaling methods (SDSM), dynamic downscaling methods, and downscaling methods combining statistics and dynamics [29,51,52]. Among the three types of methods, SDSM is easy to use and understand and has a clear physical meaning. Compared with the other two, SDSM has a simple calculation process and a small calculation load. It is a common method for downscaling GCM data [53,54]. In this paper, SDSM is used for downscaling and forecasting climate change.

The basic process of SDSM is shown in Figure 3. First, the statistical relationship is determined between observed data and NCEP reanalysis data,  $f(x)$ . Then a statistical model is established, and the accuracy of the model is tested. Finally, the statistical model is used to downscale the GCM data to obtain future meteorological data in the UYRB.

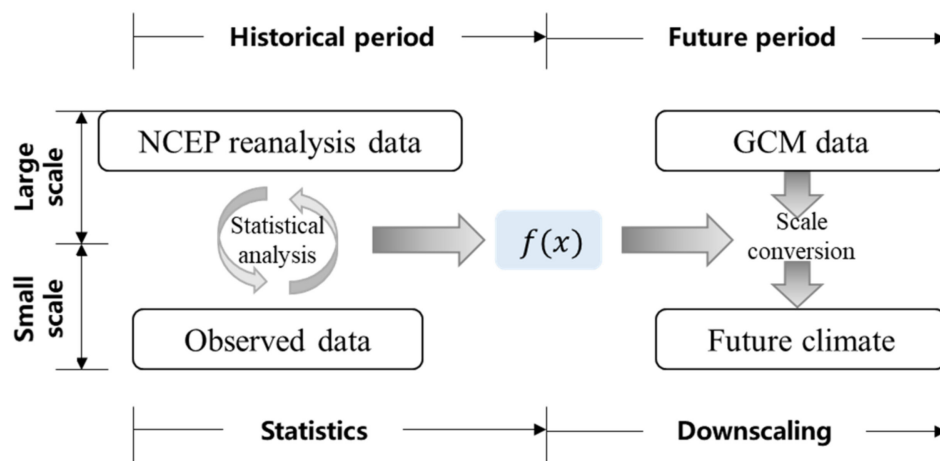


**Figure 3.** Flow chart of basic ideas of statistical downscaling method (SDSM).

SDSM 4.2 software is used in this paper [55]. In the process of establishing the statistical model, 1985–2004 is the identification period of the model, and 2005–2014 is the verification period. The established SDSM model is applied to downscale the large-scale data of CanESM5, MPI-ESM1.2, and NorESM2. The mean value of the model ensemble is used as the future climate projection in the UYRB.

NCEP reanalysis data and GCM data used by SDSM are both large-scale predictor variables. There are 23 predictor variables in total, and these are listed in Table 2.

**Table 2.** List of the 23 predictor variable IDs and corresponding names.

No.	ID	Predictor Variable	No.	ID	Predictor Variable
1	mslp	Mean sea level pressure	13	p8_u	850 hPa Zonal wind component
2	p1_f	1000 hPa Wind speed	14	p8_v	850 hPa Meridional wind component
3	p1_u	1000 hPa Zonal wind component	15	p8_z	850 hPa Relative vorticity of true wind
4	p1_v	1000 hPa Meridional wind component	16	p8zh	850 hPa Divergence of true wind
5	p1_z	1000 hPa Relative vorticity of true wind	17	p500	500 hPa Geopotential
6	p1zh	1000 hPa Divergence of true wind	18	p850	850 hPa Geopotential
7	p5_f	500 hPa Wind speed	19	prcp	Total precipitation
8	p5_u	500 hPa Zonal wind component	20	s500	500 hPa Specific humidity
9	p5_v	500 hPa Meridional wind component	21	s850	850 hPa Specific humidity
10	p5_z	500 hPa Relative vorticity of true wind	22	shum	1000 hPa Specific humidity
11	p5zh	500 hPa Divergence of true wind	23	temp	Air temperature at 2 m
12	p8_f	850 hPa Wind Speed			

### 2.3.2. Mann–Kendall Trend Test

The Mann–Kendall trend test is applied at 5% significance level to detect the significant trends in hydrometeorological time series in this study. Mann–Kendall (MK) trend test is a widely used non-parametric statistical test method. It is particularly suitable for analyzing meteorological data sequences that vary over time [56–58]. The MK trend test is usually employed to assess the presence of a monotonic trend in a time series. A monotonically increasing/decreasing trend implies that the variable consistently increases/decreases over time, but the trend may be linear or non-linear. The advantages of MK trend test over parametric tests are as follows: (1) it is applicable to various distributions and does not require the tested variable to follow a normal distribution assumption; (2) it requires a small sample size, with a minimum data sample size of 8 to 10.

Null hypothesis,  $H_0$ , of MK test assumes that there is no trend in the data  $(x_1, x_2, \dots, x_n)$ . Alternative hypothesis  $H_a$  is that the data have a monotonic trend [59].

Test statistic  $S$ :

$$S = \sum_{i=1}^{n-1} \sum_{j=i+1}^n \text{sgn}(x_j - x_i) \tag{2}$$

where  $x_j$  and  $x_i$  are the annual data values in  $j$ -th year and  $i$ -th year, respectively,  $n$  is the length of the data. The expression for the  $\text{sgn}()$  function is as follows:

$$\text{sgn}(x_j - x_i) = \begin{cases} 1 & x_j > x_i \\ 0 & x_j = x_i \\ -1 & x_j < x_i \end{cases}, \tag{3}$$

For large  $n$ , the statistic  $S$  is approximately normally distributed with mean  $E(S) = 0$  and variance  $\text{Var}(S)$  as follows:

$$\text{Var}(S) = \frac{n(n-1)(2n+5)}{18} \tag{4}$$

First, the statistical indicator,  $Z_{MK}$ , is calculated:

$$Z_{MK} = \begin{cases} \frac{S-1}{\sqrt{Var(S)}} & S > 0 \\ 0 & S = 0 \\ \frac{S+1}{\sqrt{Var(S)}} & S < 0 \end{cases}, \tag{5}$$

If  $|Z_{MK}| > Z_{1-\alpha/2}$ , the null hypothesis  $H_0$  is not acceptable, i.e., at the confidence level  $\alpha$ , there is a significant monotonic trend in the time series data. A positive value of  $Z_{MK}$  indicates an increasing trend, while a negative value indicates a decreasing trend. In this study, the significance level for the MK trend test is 5%,  $Z_{1-\alpha/2} = 1.96$ .

Then, Theil–Sen’s slope,  $\beta$ , is calculated:

$$\beta = Median\left(\frac{x_j - x_i}{j - i}\right), \forall j > i, \tag{6}$$

where  $Median()$  is the median function. Theil–Sen’s slope represents the trend magnitude of a variable per unit time [26].

### 2.3.3. Modified Mann–Kendall Trend Test

Hydrometeorological time series normally display statistically significant autocorrelation, which affects the power of MK trend test to detect trends correctly in time series data. Prewhitening is a procedure for removing autocorrelation within a given time series by adding white noise series to the original series [60]. But it has been reported that removal of positive/negative autocorrelation by prewhitening removes/adds a portion of trend, then reduces/increases the detection rate of significant trend in MK test [61,62].

Hamed and Rao proposed the modified Mann–Kendall (MMK) trend test to address autocorrelation issues with a variance correction approach [8,56,63]. The MMK trend test is applied at 5% significance level in this study.

The variance  $Var^*(S)$  in the case of autocorrelated series is as follows:

$$Var^*(S) = Var(S) \times \frac{n}{n_S^*} = \frac{n(n-1)(2n+5)}{18} \times \frac{n}{n_S^*} \tag{7}$$

where  $\frac{n}{n_S^*}$  represents a correction due to the autocorrelation in the data.  $Var(S)$  is the same as the MK test. The expression of  $\frac{n}{n_S^*}$  is as follows:

$$\frac{n}{n_S^*} = 1 + \frac{2}{n(n-1)(n-2)} \times \sum_{i=1}^{n-1} (n-i)(n-i-1)(n-i-2)\rho_S(i) \tag{8}$$

where  $\rho_S(i)$  is the autocorrelation function of the ranks of the observations.

The statistical indicator,  $Z_{MK}$  is calculated:

$$Z_{MK} = \begin{cases} \frac{S-1}{\sqrt{Var^*(S)}} & S > 0 \\ 0 & S = 0 \\ \frac{S+1}{\sqrt{Var^*(S)}} & S < 0 \end{cases}, \tag{9}$$

If  $|Z_{MK}| > Z_{1-\alpha/2}$ , the null hypothesis  $H_0$  is not acceptable, i.e., at the confidence level  $\alpha$ , there is a significant monotonic trend in the time series data. A positive value of  $Z_{MK}$  indicates an increasing trend, while a negative value indicates a decreasing trend. In this study, the significance level for the MMK trend test is 5%,  $Z_{1-\alpha/2} = 1.96$ .

The formula for Theil–Sen’s slope,  $\beta$ , is shown in Equation (6).

#### 2.3.4. Random Forest Regression Algorithm

Random forest regression model is used to identify the key climatic factors affecting surface runoff and project future surface runoff in the UYRB. Random forest is an ensemble machine learning algorithm. The random forest algorithm combines multiple weak classifiers and finally obtains the results by voting or averaging, which makes the classification or regression results of the overall model have high accuracy and generalizing performance [64].

The weak classifier used in random forest is CART decision tree, which is also called classification regression tree. When the dependent variable of the dataset is a continuous variable, the tree algorithm is a regression tree with the mean of the leaf nodes as the predicted value [65]. The random forest algorithm composed of regression trees is the random forest regression (RFR) algorithm. The algorithmic process is as follows:

- (1) Randomly sample the training dataset with dropout and construct a sub-training dataset with the same capacity as the training dataset;
- (2) Use the sub-training sample set to train a CART regression tree model. In the training process, it is necessary to randomly select some features from all feature sets and then select the optimal features according to the minimum mean square error principle;
- (3) Repeat steps (1) and (2) to generate multiple CART regression trees to form a forest;
- (4) The mean value of the prediction results of all CART regression trees is taken as the final prediction result of random forest.

It can be seen that in the process of establishing the random forest regression model, the algorithm itself has completed the screening of important features. Therefore, in this paper, the annual average temperature, annual precipitation, CDD, TR, and R×5day in the UYRB from 1985 to 2014 are taken as independent variables, and the annual surface runoff depth of the basin is taken as dependent variable. Using Python's sklearn tool library, a random forest regression model was established to calculate the importance of the independent variables to the dependent variable and identify the key climatic factors that affect the runoff of the basin.

Using 80% of the meteorological and runoff data from 1985 to 2014 in the UYRB as the training dataset, and the remaining 20% as the testing dataset. The number of weak classifiers,  $n\_estimators$ , is an important parameter of an RFR model, which has a significant impact on the fitting accuracy of the model. The model was optimized using cyclic iterative method to determine the value of  $n\_estimators$ . In this study,  $n\_estimators = 100$ , as it was found through pre-experiments that  $R^2$  and Pearson's correlation coefficient were both greater than 0.90 with  $n\_estimators = 100$ . All other parameters of the RFR model are default values. The established RFR model was applied, and the importance score of variables was calculated with function `feature_importances_`.

Before using the RFR model, we conducted a multicollinearity test on the dataset. If the variance inflation factor (VIF) value of the variable was greater than 10, it was considered that there was collinearity between the variables [66,67]. In this case, data preprocessing was necessary to remove the influence of collinearity on the identification of important variables in the RFR model.

After obtaining the key climatic factors affecting surface runoff, a new RFR model was established using the key climatic factors and surface runoff in the UYRB from 1985 to 2014. The new RFR model and future climate data were applied to predict surface runoff series in the UYRB.

#### 2.3.5. Multiple Regression Model

Multiple regression (MR) model typically refers to a linear regression model that involves two or more independent variables, aiming to explain the linear relationship between the dependent variable and multiple independent variables. Its mathematical model is expressed as follows:

$$E(y) = \beta_0 + \sum_{i=1}^n \beta_i \times x_i, \quad (10)$$

In the equation,  $y$  represents the dependent variable,  $E(y)$  denotes the estimated value of dependent variable,  $\beta_0$  is a constant term,  $n$  represents the number of independent variables,  $x_i$  represents the  $i$ -th independent variable, and  $\beta_i$  represents the coefficient of the  $i$ -th independent variable.

The response of surface runoff to climate change is nonlinear, so the accuracy of applying multiple linear regression model to predict runoff is usually not as good as that of other methods, such as neural networks, random forests, support vector machines, etc. However, the prediction results of multiple linear regression model are still able to reflect the overall trend of runoff series [68,69]. Meanwhile, because the multiple linear regression model is characterized by rapid calculation, simple operation, and intuitive results, multiple linear regression is still applied in the research of runoff prediction [70–72].

In this study, two sets of key climatic factors affecting surface runoff were identified using the Spearman rank correlation (SRC) test and random forest regression (RFR), so we needed to build a brand-new prediction model to fairly evaluate the credibility of the two sets of key climatic factors. The performance of this brand-new prediction model does not need to be particularly good; what is important is that it can reflect the trend of surface runoff. To achieve this, a multiple regression model was constructed with climatic factors in UYRB during the historical period (1985–2014) as independent variables and surface runoff depth as the dependent variable. Two multiple regression models with different input datasets were established. The multiple regression model with higher  $R^2$ , higher adjusted  $R^2$ , and smaller RMSE is considered to have used more reasonable input variables. These variables are the key climatic factors that influence surface runoff.

### 3. Results

#### 3.1. Climate Change during Historical Periods

##### 3.1.1. Temporal Variation Patterns of Precipitation and Temperature

Table A2 provides the  $Z_{MK}$  values and trend magnitudes obtained from the MK/MMK trend test for annual precipitation and annual average temperature from 1985 to 2014 at the 58 meteorological stations in the UYRB. Out of the 58 meteorological stations, the annual precipitation series of 26 stations exhibited decreasing trends, with significant (at a 5% level) decreasing trends observed at 2 stations, namely Zhanyi and Huili. Additionally, the annual precipitation of 32 stations showed increasing trends, with significant increasing trends observed at the Tuotuohe, Wudaoliang, Dari, and Suoxian stations. The trend slopes of the annual precipitation series for all stations are represented using Theil–Sen’s slope estimator. From 1985 to 2014, the trend slopes of annual precipitation in the UYRB ranged from  $-101.83$  mm/decade (Huili) to  $87.94$  mm/decade (Dongxing). The annual precipitation of the whole UYRB was calculated using the Thiessen polygon method. Figure 4 illustrates the annual precipitation in the historical period (1985–2014) of the UYRB. The multi-year mean annual precipitation is  $807.03$  mm, with the maximum precipitation recorded at  $923.26$  mm in 1998 and the minimum at  $707.62$  mm in 2006. The annual precipitation in the historical period of UYRB exhibits a slightly increasing trend, with a trend slope of  $10.44$  mm/decade.

Regarding the annual average temperature, out of the 58 meteorological stations, except for Guiyang station, where the temperature shows a significant (at a 5% level) decrease, the temperature at the remaining 57 stations exhibited increasing trends. Among them, 53 stations showed significant (at a 5% level) warming trends. The trend slopes of the annual average temperature ranged from  $-0.42$  °C/decade (Guiyang) to  $0.99$  °C/decade (Leibo). Figure 5 illustrates the annual average temperature in the historical period (1985–2014) in the UYRB, which showed an increasing trend. The maximum temperature recorded was  $12.45$  °C in 2006, which coincided with the year of the minimum precipitation. The minimum temperature occurred in 1992, with a value of  $10.64$  °C. The  $Z_{MK}$  value for the annual average temperature in the UYRB is  $4.14$ , indicating a significant increasing trend at a 5% level. The warming trend slope is  $0.42$  °C/decade.

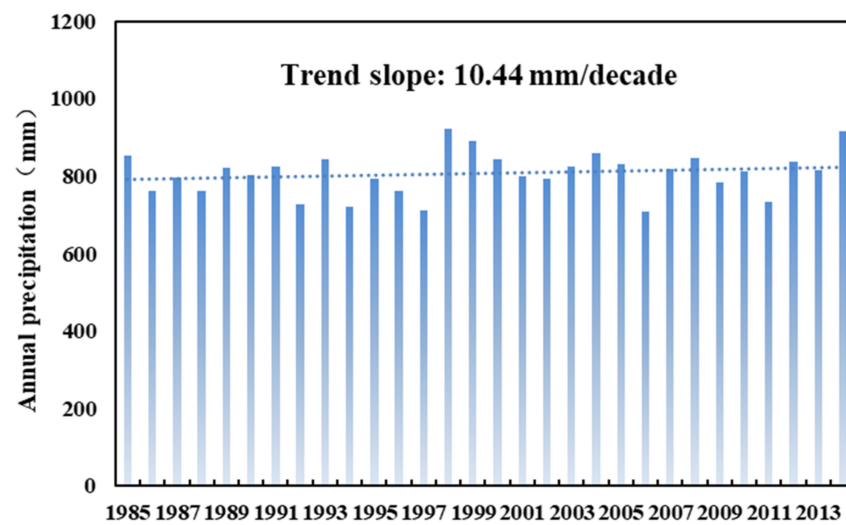


Figure 4. Annual precipitation series of the UYRB during 1985–2014.

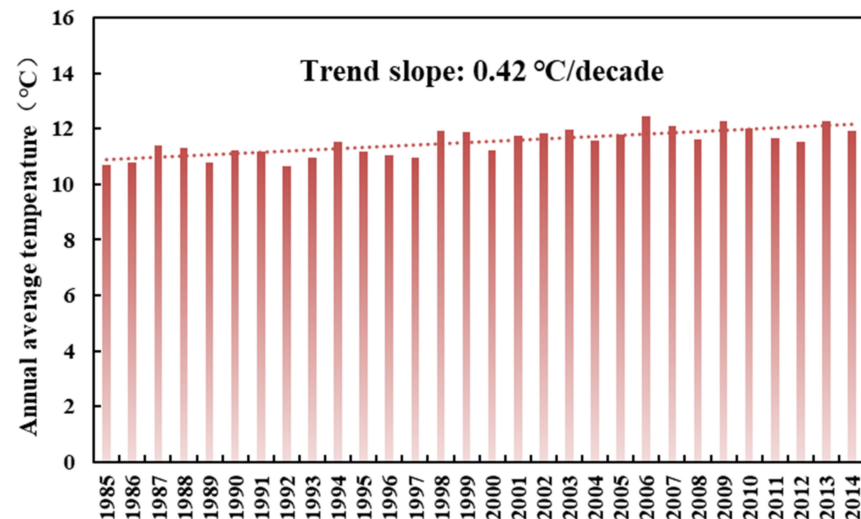


Figure 5. Annual average temperature series of the UYRB during 1985–2014.

### 3.1.2. Spatial Variation Patterns of Precipitation and Temperature

The spatial patterns of the trend slopes in annual precipitation (1985–2014) in the UYRB are shown in Figure 6. In the western high-altitude regions, there was a general increasing trend in annual precipitation, with an increase ranging from 0 to 60 mm/decade. Moreover, the closer to the source of the Jinsha River basin, the greater the magnitude of the increase in annual precipitation. Precipitation in the Jialing River basin and Mintuo River basin also increased. Annual precipitation decreased in the southwestern part of the UYRB. In particular, the lower reaches of the Jinsha River basin showed the most pronounced decrease in precipitation. The annual precipitation series of Zhanyi and Huili decreased significantly (at a 5% level), with slopes of  $-90.75$  mm/decade and  $-101.83$  mm/decade, respectively.

The spatial patterns of the trend slopes in annual average temperature from 1985 to 2014 in the UYRB are depicted in Figure 7. It can be observed that almost the entire UYRB exhibits significant warming trends, with localized areas in the southeast showing decreasing temperature trends. Across the whole UYRB, the warming trend slope decreases from northwest to southeast, and the significance of the trend gradually diminishes. In the high-altitude regions of the northwest, the warming magnitude ranges from 0.4 to 0.8 °C/decade, which is higher than that in the eastern and southeastern parts of the

UYRB. Near Guiyang, the trend of the annual average temperature shifts from an increasing trend to a decreasing trend, with a slope of  $-0.42\text{ }^{\circ}\text{C}/\text{decade}$  for Guiyang.

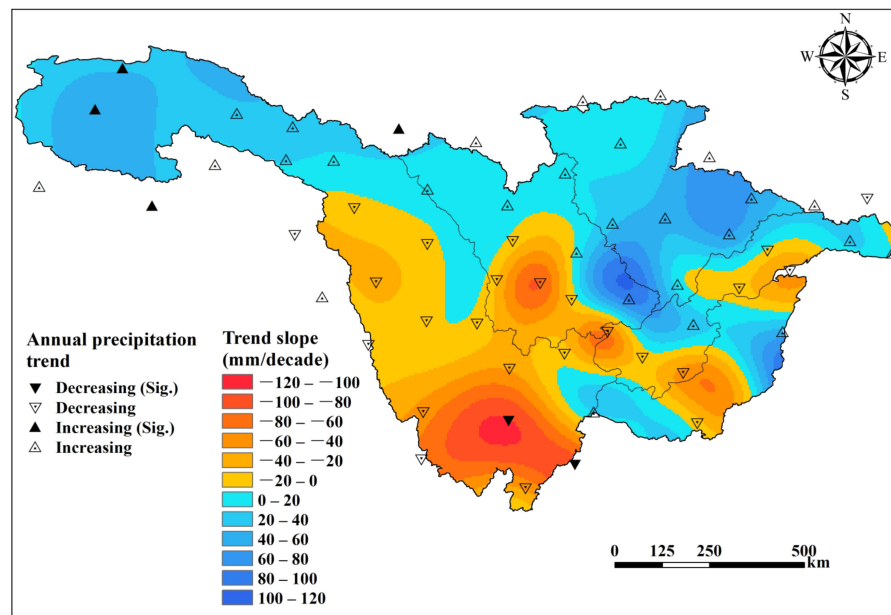


**Figure 6.** Spatial distribution of annual precipitation trend slope in the UYRB (1985–2014). Note: “Sig.” means significant at 5% level. Upward solid triangles represent significant increasing trends. Upward hollow triangles represent an increasing trend that is not significant. A downward solid triangle represents a significant downward trend. Downward hollow triangles represent a non-significant downward trend.

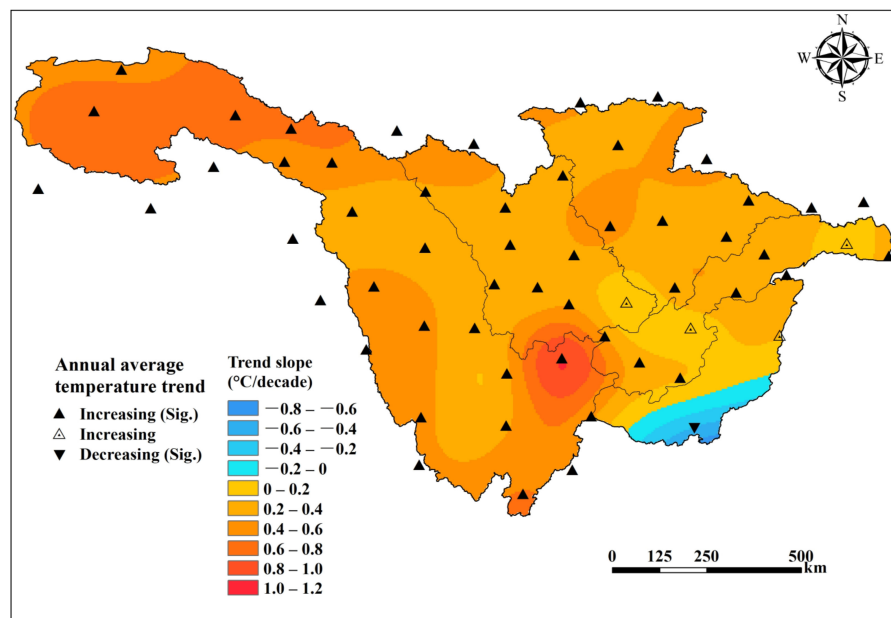


**Figure 7.** Spatial distribution of annual average temperature trend slope in the UYRB (1985–2014). Note: “Sig.” means significant at 5% level. Upward solid triangles represent significant increasing trends. Upward hollow triangles represent an increasing trend that is not significant. A downward solid triangle represents a significant downward trend. Downward hollow triangles represent a non-significant downward trend.

### 3.2. Identification and Verification of Statistical Downscaling Model

Figure 8 presents the simulation results of the statistical downscaling model (SDSM) during the identification period (1985–2004) and verification period (2005–2014). It can be observed that SDSM performs better at simulating the temperature compared to the precipitation. In each month, the simulated temperature values by SDSM closely match the observed values, capturing the dynamic characteristics of the temperature in the UYRB. However, the simulated rainfall tends to be overestimated, especially during the rainy season (from May to October). In terms of dynamic characteristics, the simulated results can also capture the variability of precipitation in the UYRB well.

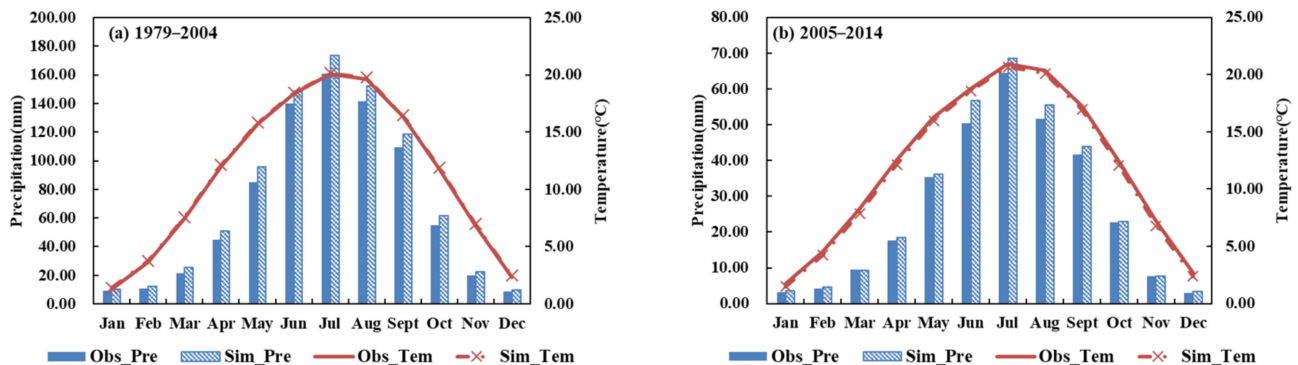


**Figure 8.** Simulation results of SDSM during identification (a) and verification (b) periods. Note: Obs\_Pre is the observed precipitation, Sim\_Pre is the simulated precipitation, Obs\_Tem is the observed temperature, and Sim\_Tem is the simulated temperature.

The simulation results of the annual precipitation and temperature by SDSM during the identification and verification periods are shown in Figure 9. At the annual time scale, the SDSM demonstrates better accuracy in simulating the temperature than the precipitation, and the simulated precipitation values exceed the observed values, which is consistent with the monthly scale simulation results (Figure 8). Figure 9 illustrates the linear trends of precipitation and temperature. It can be observed that, both in the identification and verification periods, the trends of the simulated values by the SDSM align with the observed values. In the identification period, both precipitation and temperature show an increasing trend. In the verification period, the precipitation exhibits an increasing trend, while the temperature shows a decreasing trend. This discrepancy with the MK/MMK trend test of the annual average temperature in the UYRB from 1985 to 2014 may be attributed to the fact that the verification period is too short, at only 10 years (2005–2014). Hydro-meteorological series are usually highly random over a short period, which greatly affects the accuracy of trend analysis. The trend of temperature we obtained is a short-period trend.

### 3.3. Future Climate Change in the Upper Yangtze River Basin

#### 3.3.1. Temporal Variation Patterns of Future Precipitation and Temperature

Figure 10 represents the annual precipitation and annual average temperature series for the historical (1985–2014) and future (mid-term: 2036–2065, long term: 2071–2100) periods in the UYRB. The results of the MK trend test and trend slopes for future precipitation are provided in Table 3.

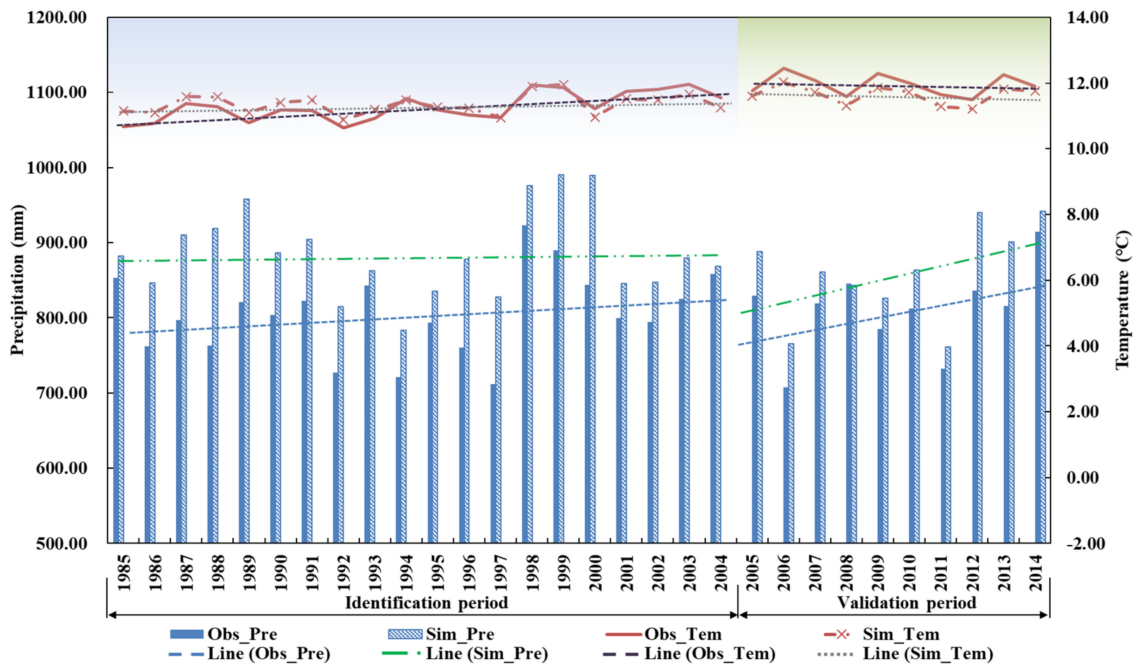


Figure 9. Simulation results and linear trends of annual precipitation and temperature over the UYRB during 1985–2014. Note: Obs\_Pre is the observed precipitation, Sim\_Pre is the simulated precipitation, Obs\_Tem is the observed temperature, and Sim\_Tem is the simulated temperature.

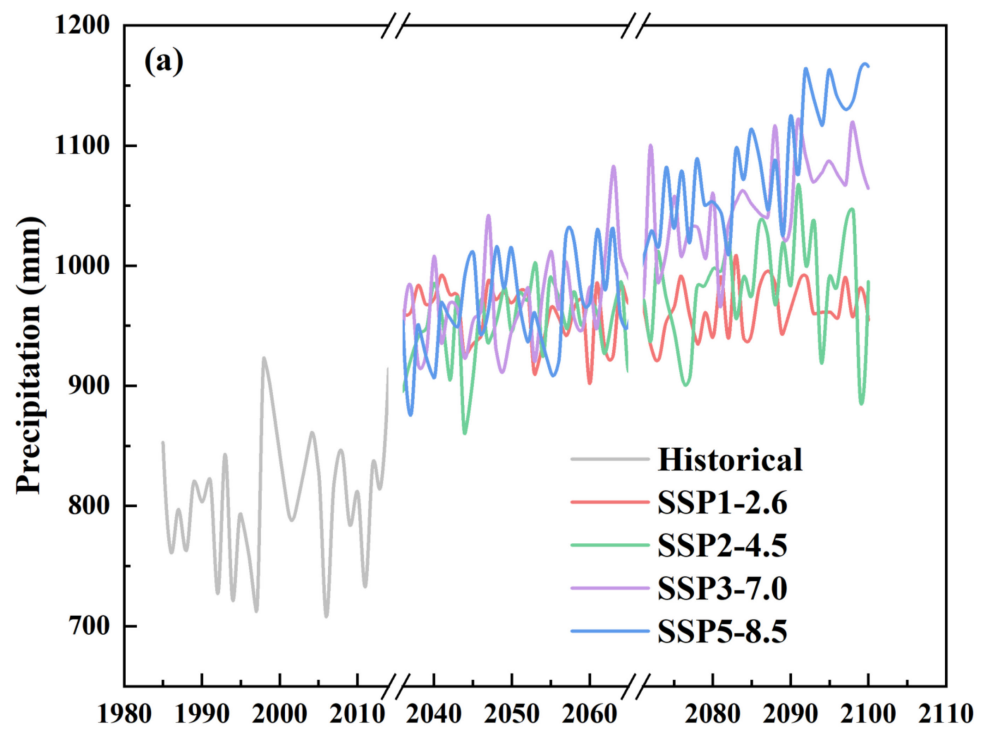


Figure 10. Cont.

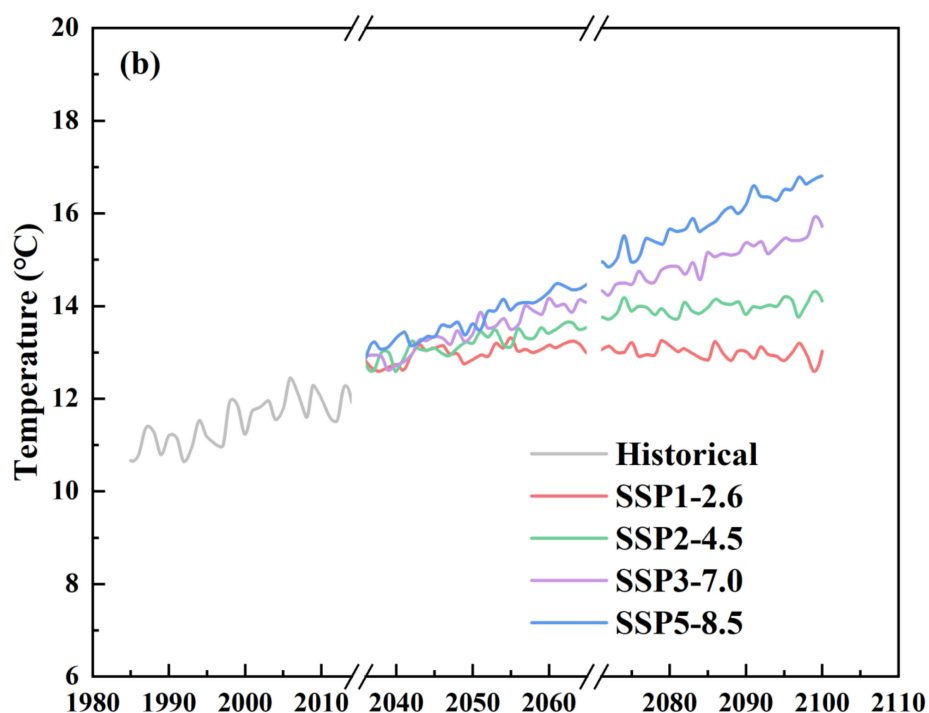


Figure 10. Prediction results of (a) future annual precipitation and (b) annual average temperature for the whole UYRB.

Table 3. Projected mean annual precipitation (MAP) change in different future periods in the UYRB.

	1985–2014			2036–2065			2071–2100		
	MAP (mm)	Z <sub>MK</sub>	Slope (mm/Decade)	MAP (mm)	Z <sub>MK</sub>	Slope (mm/Decade)	MAP (mm)	Z <sub>MK</sub>	Slope (mm/Decade)
Historical period	807.03	0.82	10.44						
SSP1-2.6				959.84	−0.89	−5.30	963.92	1.14	7.08
SSP2-4.5				950.54	1.61	12.08	984.64	<b>2.00</b>	16.68
SSP3-7.0				968.68	<b>2.18</b>	17.06	1051.63	<b>2.34</b>	29.17
SSP5-8.5				965.79	1.93	12.37	1085.30	<b>4.67</b>	47.93

Note: The “**Bold**” denotes a significant trend (at 5% level), |Z<sub>MK</sub>| > 1.96. The “*italics*” represent the MMK values of time series with autocorrelation.

From Figure 10a, it can be observed that the mean annual precipitation (MAP) for all four future SSP scenarios is higher than that in the historical period. In the mid-term (2036–2065), the MAP values of the four scenarios are close, as is shown in Figure 10a, with the four curves close together and overlapping with each other. The MAP of SSP1-2.6 in the mid-term (2036–2065) is 959.84 mm, which is an increase of 18.93% compared to the historical period (1985–2014). The MAP of SSP2-4.5 in the mid-term is 950.54 mm (an increase of 17.78%), SSP3-7.0 is 968.68 mm (an increase of 20.03%), and SSP5-8.5 is 965.79 mm (an increase of 19.67%) (Table 3). In the mid-term (2036–2065), SSP1-2.6 shows a decreasing trend in precipitation with a slope of −5.30 mm/decade. The other three scenarios show an increasing trend in precipitation. Under SSP3-7.0, precipitation increases significantly (at a 5% level) with a slope of 17.06 mm/decade.

In the long term (2071–2100), the MAP values of the four scenarios appear significantly different. In Figure 10a, the four curves in the long term are spread out, and the precipitation curve is more upward for a high radiative forcing value. The maximum MAP is 1085.30 mm under SSP5-8.5, and the minimum is 963.92 mm under SSP1-2.6. In the long term (2071–2100), the precipitation curves of SSP2-4.5, SSP3-7.0, and SSP5-8.5 have a clear increasing trend, except for SSP1-2.6. The slope increases as the radiative forcing increases.

The results in Table 3 show that the precipitation increases significantly (at a 5% level) under all four future scenarios.

The precipitation-increasing trends of SSP2-4.5, SSP3-7.0, and SSP5-8.5 are significant (at a 5% level). The trend slopes in descending order are SSP5-8.5 (47.93 mm/decade), SSP3-7.0 (29.17 mm/decade), SSP2-4.5 (16.68 mm/decade), and SSP1-2.6 (7.08 mm/decade).

From Figure 10b, it can be seen that under all four future scenarios, the mean annual average temperature (MAT) values in the UYRB are higher than those in the historical period. The MAT values increase with increasing radiative forcing. The temperature curves in Figure 10b can be divided into three categories.

The first category: Temperature curves continue to increase in both the mid-term (2036–2065) and the long term (2071–2100), and the slopes are relatively stable. The temperature curves of SSP3-7.0 and SSP5-8.5 belong to the first category. As can be seen in Table 4, the temperature of SSP3-7.0 increases significantly (at a 5% level) in both the mid-term and the long term. The MAT of the mid-term is 13.47 °C, which is an increase of 17.03% compared with the historical period. The long term MAT is 15.00 °C, which is an increase of 30.32% compared with the historical period. The trend slopes for the mid-term and long term under SSP3-7.0 are close to each other, with values of 0.47 and 0.45 °C/decade, respectively. The temperature of SSP5-8.5 shows a significant increasing trend (at a 5% level) both in the mid-term and the long term. The MAT values of the mid-term and long term are 13.73 °C (an increase of 19.29%) and 15.88 °C (an increase of 37.97%), respectively. The temperature slopes for the mid-term and long term under SSP5-8.5 are 0.54 °C/decade and 0.67 °C/decade.

**Table 4.** Projected mean annual temperature (MAT) change in different future periods in the UYRB.

	1985–2014			2036–2065			2071–2100		
	MAT (°C)	Z <sub>MK</sub>	Slope (°C/Decade)	MAT (°C)	Z <sub>MK</sub>	Slope (°C/Decade)	MAT (°C)	Z <sub>MK</sub>	Slope (°C/Decade)
Historical period	11.51	<b>4.14</b>	0.42						
SSP1-2.6				12.98	<b>3.71</b>	0.16	13.00	−1.75	−0.05
SSP2-4.5				13.20	<b>5.39</b>	0.29	13.97	<b>2.82</b>	0.10
SSP3-7.0				13.47	<b>6.07</b>	0.47	15.00	<b>6.53</b>	0.45
SSP5-8.5				13.73	<b>6.60</b>	0.54	15.88	<b>6.64</b>	0.67

Note: The “**Bold**” denotes a significant trend (at 5% level), |Z<sub>MK</sub>| > 1.96. The “*italics*” represent the MMK values of time series with autocorrelation.

The second category: Temperature curves increase in both the mid-term (2036–2065) and long term (2071–2100), but the slope in the long term is obviously smaller than that in the mid-term. The temperature curve of SSP2-4.5 belongs to the second category. Table 4 shows that the temperature under SSP2-4.5 increases significantly (at a 5% level) in both the mid-term and the long term. The MAT of the mid-term is 13.20 °C, which is an increase of 14.68% compared with the historical period. The long term MAT is 13.97 °C, which is an increase of 21.37% compared with the historical period. The slope is 0.29 °C/decade in the mid-term and 0.10 °C/decade in the long term, which is a decrease of 65.52% compared to the mid-term.

The third category: Temperature shows an increasing trend in the mid-term (2036–2065) and a decreasing trend in the long term (2071–2100). The temperature curve of SSP1-2.6 belongs to the third category. Table 4 shows that the temperature under SSP1-2.6 increases significantly (at a 5% level) in the mid-term with a MAT value of 12.98 °C, which is an increase of 12.77% compared to the historical period. The slope in the mid-term is 0.16 °C/decade. In the long term, the temperature shows a decreasing trend. The MAT in the long term is 13.00 °C, which is an increase of 12.95% compared to the historical period. The temperature slope in the long term is −0.05 °C/decade.

### 3.3.2. Spatial Variation Patterns of Future Precipitation and Temperature

The spatial distributions of the mean annual precipitation in the future periods over the UYRB are shown in Figure 11. From northwest to southeast, the annual precipitation increases under all four scenarios. With increasing radiative forcing, the area of the humid region in UYRB expands, and the semi-humid and semi-arid regions decrease.

In the mid-term (2036–2065), the spatial patterns of precipitation under the four scenarios are the same: see the left column of Figure 11 (Figure 11a–d). Here, SSP1-2.6 is used as an example for the analysis (Figure 11a), and the analysis of the other three scenarios is omitted. Compared with the historical period (1985–2014), the upstream region of the Mintuo River basin changes from a semi-humid region to a humid region, which increases the total area of the humid region in the UYRB. Within the humid region, the area of the heavy precipitation region with precipitation greater than 1200 mm increases. Almost all of the Yibin–Yichang River basin becomes a heavy precipitation region, as do the lower Jialing River basin, the lower Wu River basin, and the lower Jinsha River basin. Semi-arid regions are distributed in the upstream region of the Jinsha River basin, and the area of semi-arid regions in the mid-term is smaller than that in the historical period.

In the long term (2071–2100), the total area of the humid regions in the UYRB is greater than that in the mid-term (2036–2065), as shown in the right column of Figure 11 (Figure 11e–h). The spatial distribution patterns of the mean annual precipitation are similar under the SSP3-7.0 and SSP5-8.5 scenarios. The area of humid regions under the high radiative forcing scenario is larger than that under the low radiative forcing scenario. The middle reaches of the Jinsha River basin change from a semi-humid region to a humid region, and the area of the heavy precipitation region increases with the increasing radiative forcing. In contrast to SSP1-2.6 and SSP2-4.5 scenarios (Figure 11e,f), under SSP3-7.0 and SSP5-8.5 (Figure 11g,h), almost the whole Wu River basin turns into a heavy precipitation region.

Figure 12 shows the spatial distribution of the trend slopes for the future annual precipitation of the UYRB. The results of the MK/MMK trend test and trend slopes can be found in Table A3. In the mid-term (2036–2065), the spatial pattern of precipitation slopes under SSP1-2.6 is different from the other three scenarios, as shown in the left column of Figure 12 (Figure 12a–d). Under SSP1-2.6, precipitation decreases in the lower Jinsha River basin, the lower Mintuo River basin, the Jialing River basin, and the Yibin–Yichang River basin. Precipitation increases in the other regions of the UYRB. The decreasing regions are indicated in yellow and orange, and the increasing regions are blue in Figure 12a. Under SSP2-4.5, SSP3-7.0, and SSP5-8.5 (Figure 12b–d), precipitation increases significantly (at 5% level) in most parts of the UYRB, including the upper and lower parts of the Jinsha River basin, the Yibin–Yichang River basin, and the Wu River basin. In the Jialing River basin and the upper Mintuo River basin, precipitation increases under SSP3-7.0 and SSP5-8.5 (Figure 12c,d) and decreases under SSP2-4.5 (Figure 12b).

In the long term (2071–2100), precipitation increases in most parts of the UYRB under all four scenarios, as shown in the right column of Figure 12 (Figure 12e–h). Under SSP1-2.6, precipitation decreases only in the upper Jinsha River basin, the Wu River basin, and the Yibin–Yichang River basin and increases in the remaining regions. The spatial pattern of the precipitation slope under SSP1-2.6 in the long term is the opposite of that in the mid-term. Under SSP2-4.5, precipitation decreases in the middle reaches of the Jinsha River basin and the middle reaches of the Wu River basin and increases in the remainder of the UYRB. Under SSP3-7.0 and SSP5-8.5, precipitation increases significantly (at a 5% level) over the vast majority of the UYRB. The regions with decreasing precipitation are small in size, and they are only distributed within the lower Jinsha River basin, the lower Mintuo River basin, and the Wu River basin.

The spatial distribution of the mean annual average temperature in the future over the UYRB is depicted in Figure 13. Under the four scenarios, the mean annual average temperature in the UYRB increases along the northwest to southeast direction, and this spatial pattern is shown in Figure 13 as a change in color from blue to red.

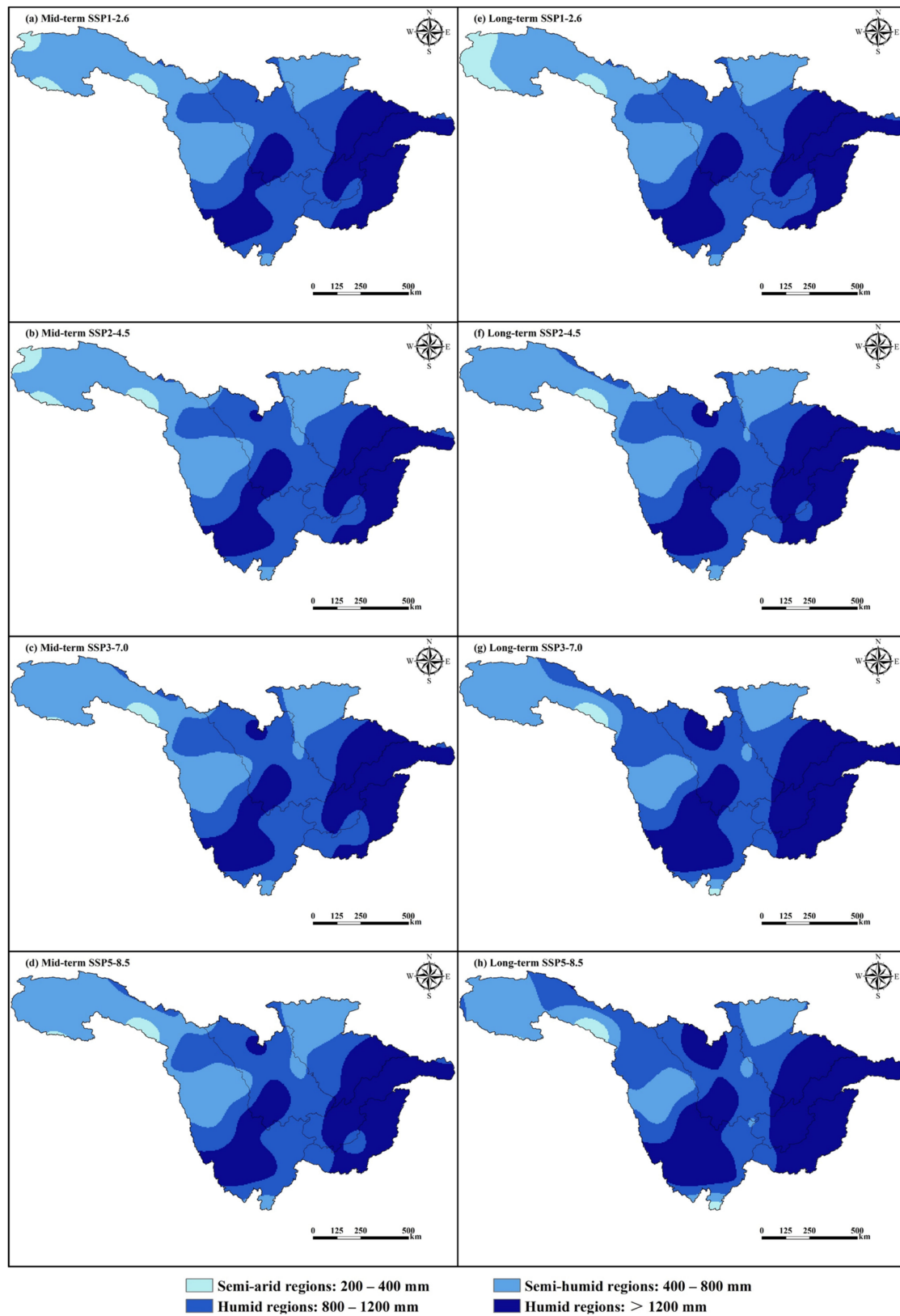


**Figure 11.** Spatial distributions of mean annual precipitation (mm) over the UYRB. The left column is mid-term (2036–2065): (a) mid-term SSP1-2.6, (b) mid-term SSP2-4.5, (c) mid-term SSP3-7.0, (d) mid-term SSP5-8.5. The right column is long term (2071–2100): (e) long term SSP1-2.6, (f) long term SSP2-4.5, (g) long term SSP3-7.0, (h) long term SSP5-8.5.

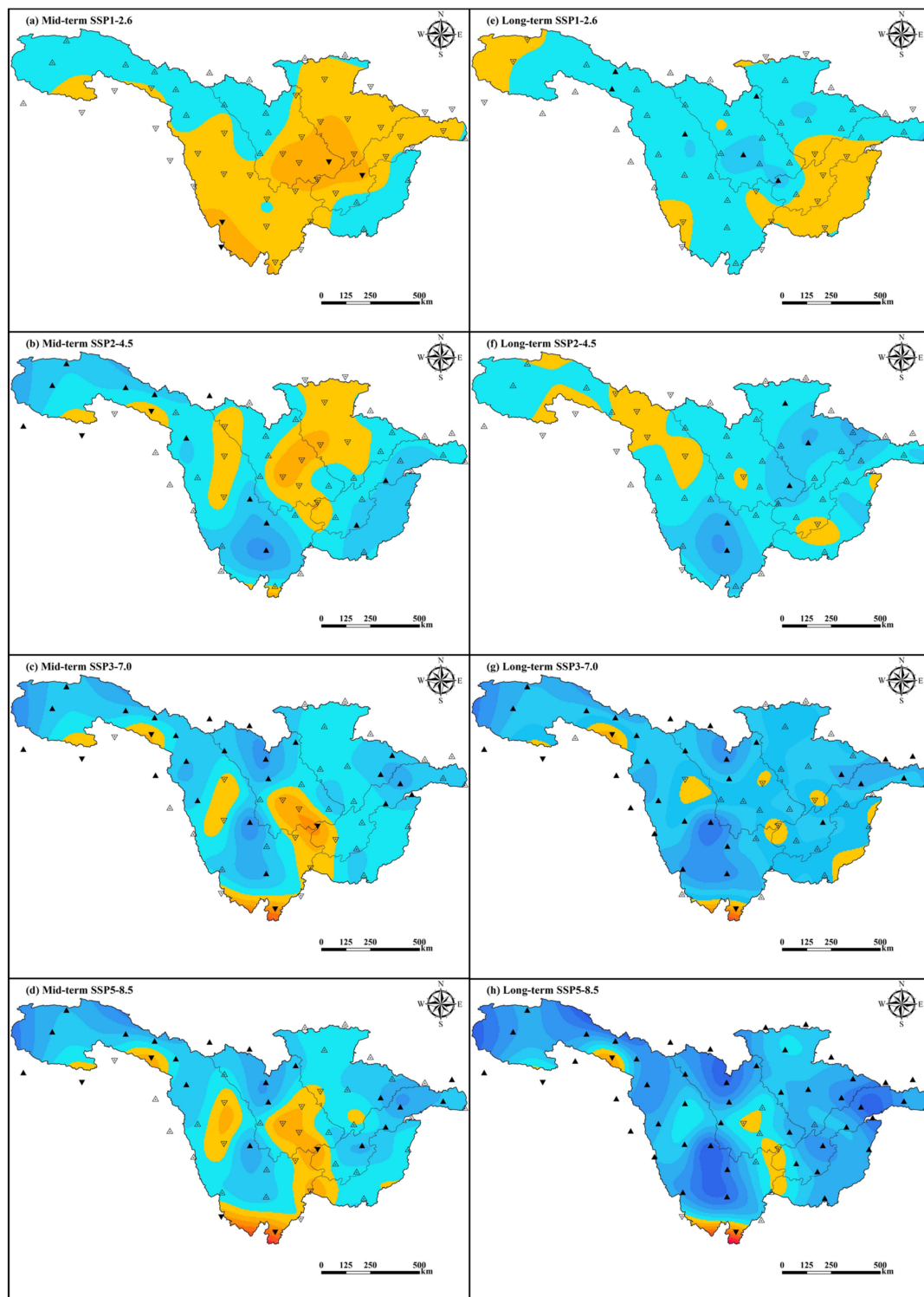


**Figure 12.** Spatial distributions of trend and significance and trend slope in annual precipitation over UYRB. The left column is mid-term (2036–2065): (a) mid-term SSP1-2.6, (b) mid-term SSP2-4.5, (c) mid-term SSP3-7.0, (d) mid-term SSP5-8.5. The right column is long term (2071–2100): (e) long term SSP1-2.6, (f) long term SSP2-4.5, (g) long term SSP3-7.0, (h) long term SSP5-8.5.

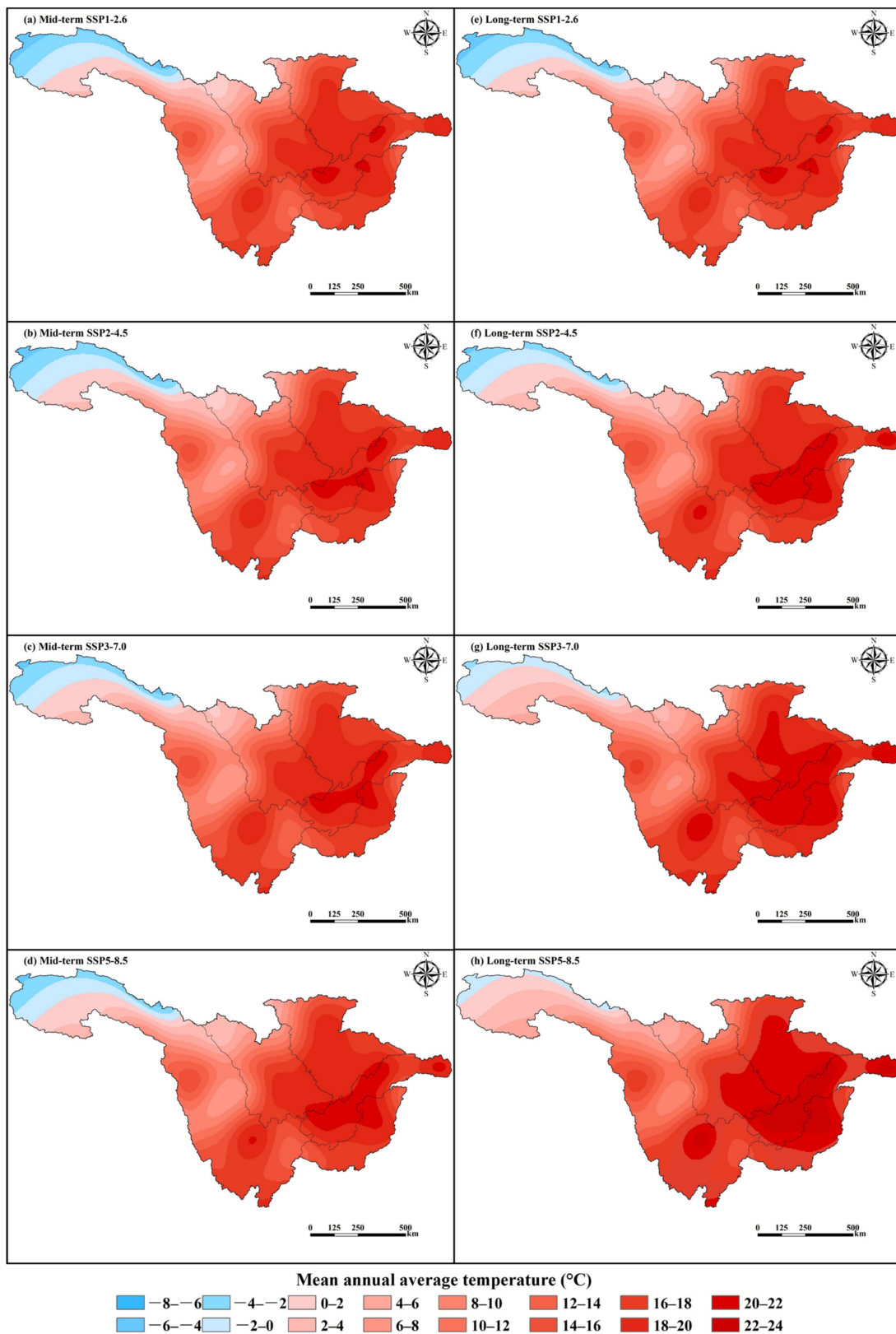


**Figure 13.** Spatial distributions of mean annual average temperature (°C) over the UYRB. The left column is mid-term (2036–2065): (a) mid-term SSP1-2.6, (b) mid-term SSP2-4.5, (c) mid-term SSP3-7.0, (d) mid-term SSP5-8.5. The right column is long term (2071–2100): (e) long term SSP1-2.6, (f) long term SSP2-4.5, (g) long term SSP3-7.0, (h) long term SSP5-8.5.

In the mid-term (2036–2065), the spatial patterns of temperature under the four scenarios are the same, as seen in the left column of Figure 13 (Figure 13a–d). The area of the cold regions with temperatures less than 0 °C (indicated in blue color) in the northwestern part of the UYRB shrinks slightly as the radiative forcing increases. The area of the high-temperature regions with temperatures greater than 20 °C increases slightly but remains mainly within the Yibin–Yichang River basin.

In the long term (2071–2100), the area of the cold regions decreases and the area of the high-temperature regions increases dramatically as the radiative forcing increases. The area of high-temperature regions under SSP5-8.5 is the largest and is distributed in the Mintuo River basin, Jialing River basin, Yibin–Yichang River basin, and Wu River basin. Under SSP1-2.6, the spatial pattern of temperature in the long term is almost the same as in the mid-term (Figure 13a,e). Under SSP2-4.5, SSP3-7.0, and SSP5-8.5 (Figure 13f–h), the area of the cold regions in the long term is smaller than that in the mid-term, and the area of the high-temperature regions is larger.

The trend slopes of annual average temperature in the future for the four scenarios in the UYRB can be seen in Figure 14 and Table A4. In different future periods, temperature over the entire UYRB under all four scenarios increases significantly (at a 5% level), except for SSP1-2.6 in the long term (Figure 14e). Under SSP2-4.5, the slope in the long term is smaller than that in the mid-term. In the mid-term, the temperature increases significantly (at a 5% level) in the whole UYRB under SSP2-4.5 (Figure 14b), while in the long term (Figure 14f), the increasing temperature trends are not significant in the Mintuo River basin, Jialing River basin, or Yibin–Yichang River basin. Under SSP3-7.0, the slopes in the Jialing River basin, Mintuo River basin, and Yibin–Yichang River basin in the long term (Figure 14g) are smaller than those in the mid-term (Figure 14c). Under SSP5-8.5, the slope in the long term (Figure 14h) is greater than that in the mid-term (Figure 14d).

### 3.4. The Influence of Climate Change on Surface Runoff

#### 3.4.1. Key Climatic Factors Affecting Surface Runoff

In the historical period (1985–2014), the annual surface runoff depth in UYRB showed a decreasing trend (Figure 15). The trend test yielded a result of  $Z_{MK} = -1.41$ , indicating a non-significant decreasing trend with a slope of  $-14.43$  mm/decade. In the historical period, the mean annual surface runoff (MAR) depth in the UYRB was 418.62 mm, with a maximum value of 517.63 mm observed in 1998, which coincided with a year of heavy rainfall and resulted in a severe flood disaster in the Yangtze River basin. The minimum value of 284.60 mm was recorded in 2006, which was a year with the lowest precipitation and highest temperature. This indicates that extreme weather events may have an impact on the surface runoff in the UYRB.

We considered annual precipitation, annual average temperature, number of tropical nights (TR), maximum consecutive 5-day precipitation ( $R \times 5$ day), and consecutive dry days (CDD) as the climatic factors to be identified, using the Spearman rank correlation (SRC) test and the random forest regression (RFR) model to identify the key climatic factors influencing surface runoff depth. The Spearman rank correlation test is applied at a 5% level of significance, and it assesses the strength of the relationship between different factors and surface runoff by examining the magnitude of the correlation coefficients. The random forest regression model calculates the importance score of each climatic factor in relation to surface runoff. The sum of the importance scores of all factors is 1, with higher importance score values indicating greater significance of the factor in influencing surface runoff. Before the climatic factor datasets were input into the RFR model, the datasets were analyzed for multicollinearity. If the variance inflation factor (VIF) value of the variable was greater than 10, it was considered that there was collinearity between the variables. The results of the correlation test and importance analysis can be found in Table 5.

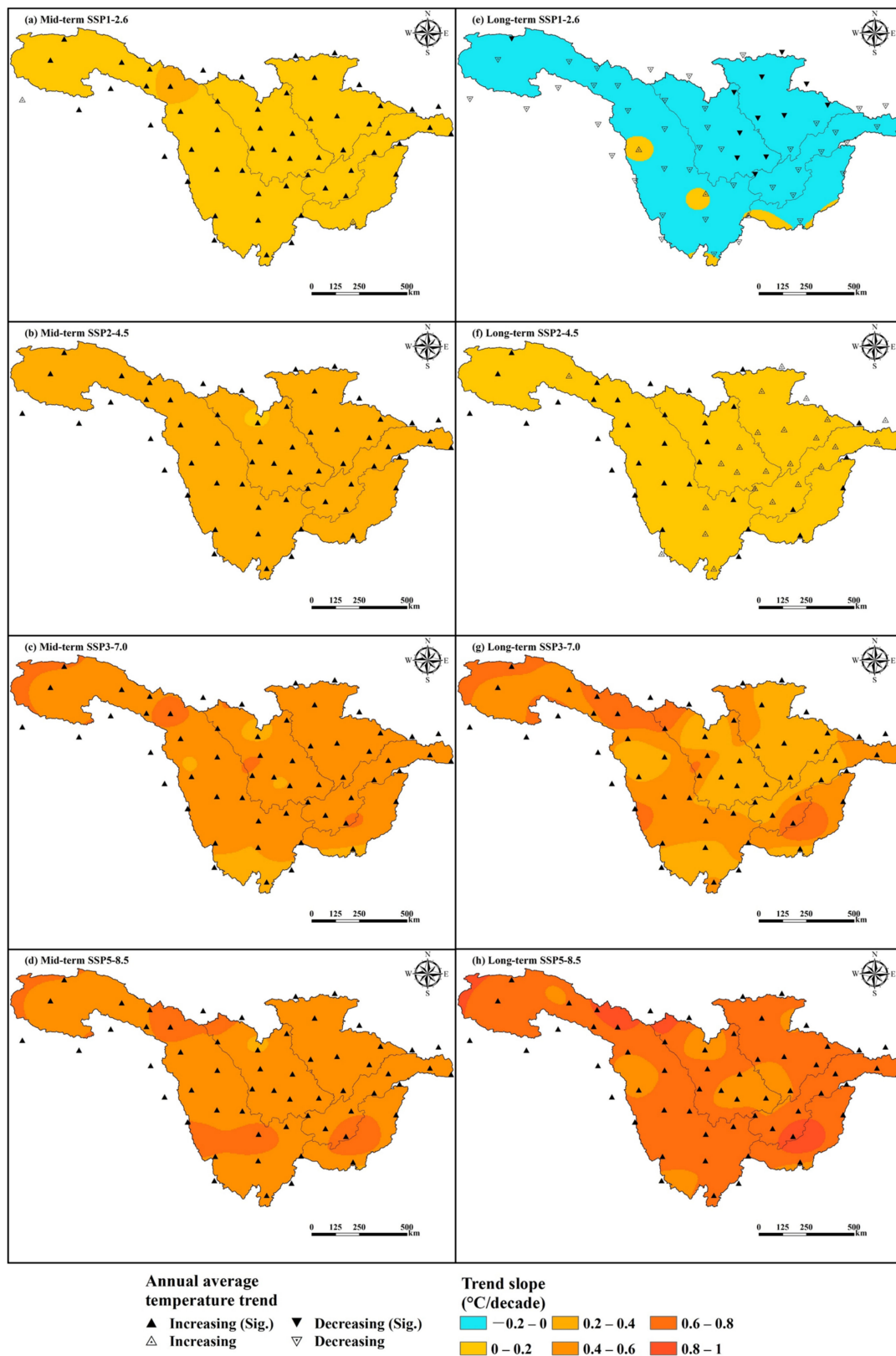


**Figure 14.** Spatial distributions of trend and significance and trend slope in annual average temperature over UYRB. The left column is mid-term (2036–2065): (a) mid-term SSP1-2.6, (b) mid-term SSP2-4.5, (c) mid-term SSP3-7.0, (d) mid-term SSP5-8.5. The right column is long term (2071–2100): (e) long term SSP1-2.6, (f) long term SSP2-4.5, (g) long term SSP3-7.0, (h) long term SSP5-8.5.

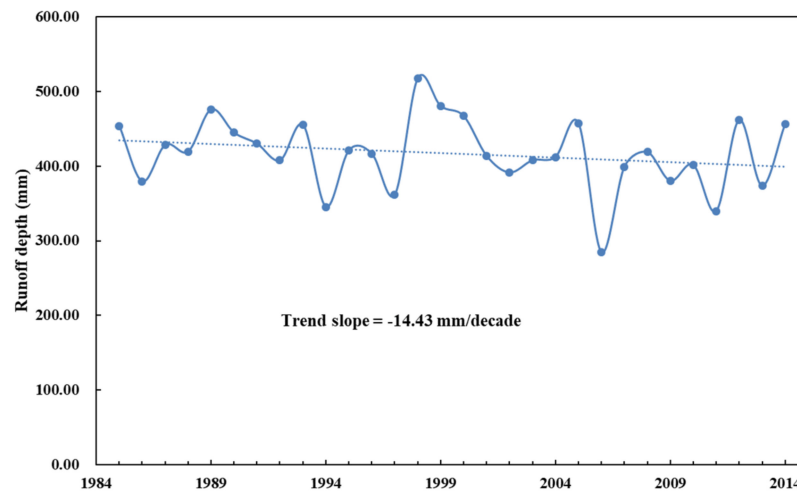


Figure 15. Annual surface runoff depth of UYRB during 1985–2014.

Table 5. Results of correlation test and importance analysis.

Methods	Index	Climatic Factors				
		Precipitation	R×5day	Temperature	CDD	TR
Multicollinearity analysis	VIF	2.17	2.02	4.45	1.10	4.55
RFR	Importance score	0.57	0.16	0.12	0.08	0.07
SRC	Correlation coefficient	<b>0.75</b>	<b>0.46</b>	−0.31	0.15	− <b>0.44</b>

Note: The “**Bold**” represents a significant result at the 5% level.

The results of the SRC test indicate a strong positive correlation between precipitation and surface runoff, with the correlation coefficient being the highest at 0.75. The R×5day shows a moderate positive correlation with surface runoff (correlation coefficient of 0.46), while the CDD exhibits a very weak positive correlation with surface runoff (correlation coefficient of 0.15). The mean annual average temperature and TR are negatively correlated with surface runoff, with correlation coefficients of −0.31 (weak correlation) and −0.44 (moderate correlation), respectively. At a significance level of 5%, the relationships between annual precipitation, R×5day, TR, and surface runoff are significant and are the key climatic factors influencing surface runoff.

The VIF values for all variables are less than 10, indicating that there is no multicollinearity affecting the importance analysis results of the RFR model. The importance analysis results reveal that precipitation has the greatest importance in explaining the variation in surface runoff, with an importance score of 0.57. In descending order of importance, the factors are ranked as follows: annual precipitation > R×5day > annual average temperature > CDD > TR. The combined importance of precipitation, R×5day, and temperature reaches 0.85, indicating a high explanatory power for surface runoff. On the other hand, CDD and TR have a minor impact on surface runoff.

The two methods, SRC and RFR, identify slightly different key climatic factors that influence surface runoff. Both the SRC and RFR results confirm that precipitation and R×5day are crucial factors affecting surface runoff. The SRC identifies the third key factor as TR, whereas the RFR identifies annual temperature as the third key factor. These variations in results may arise from differences in the underlying algorithms and statistical approaches used by the two methods. Nonetheless, the consensus on the importance of precipitation and R×5day highlights their significant role in determining surface runoff patterns.

### 3.4.2. Changes in Future Surface Runoff

Since there are differences in the conclusions drawn from the Spearman rank correlation (SRC) test and the random forest regression (RFR) model, two MR models, MR<sub>SRC</sub> and

MR<sub>RFR</sub>, were constructed, and the model with the higher simulation accuracy was considered to have used more reasonable input variables. The two MR models' parameters and indicators can be found in Table 6, and the simulation results are illustrated in Figure 16.

**Table 6.** Parameters and indicators of two multiple regression models.

Models	y	x	$\beta_i$	$\beta_0$	R <sup>2</sup>	Adjusted R <sup>2</sup>	RMSE
MR <sub>SRC</sub>	Surface runoff	Pre	0.64	−28.62	0.78	0.75	23.99
		R×5day	−0.25				
		TR	−1.47				
MR <sub>RFR</sub>	Surface runoff	Pre	0.73	278.24	0.82	0.80	21.29
		R×5day	0.49				
		Tem	−41.21				

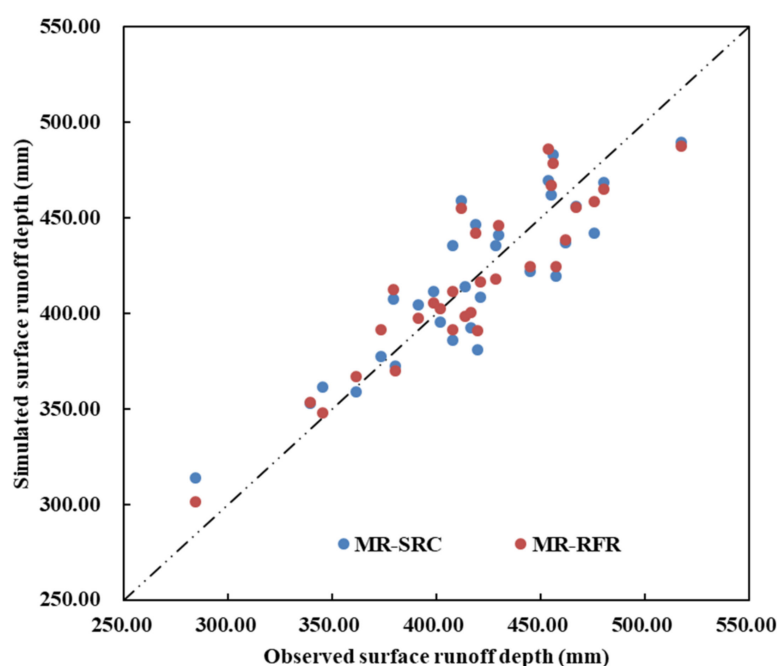


**Figure 16.** Comparison of prediction results between MR<sub>SRC</sub> and MR<sub>RFR</sub> models.

Table 6 shows that the R<sup>2</sup> and adjusted R<sup>2</sup> values of MR<sub>RFR</sub> are higher than those of MR<sub>SRC</sub>, and the RMSE is smaller. Figure 16 also demonstrates that the predicted values of MR<sub>RFR</sub> are closer to the 1:1 line. This means that the input variables of MR<sub>RFR</sub> are more reasonable. The key climatic factors affecting surface runoff are annual precipitation, R×5day, and annual average temperature. The key climatic factors and surface runoff data in the UYRB from 1985 to 2014 were used to build a new RFR model. The new RFR model was utilized to predict future surface runoff by inputting climate data from the four future scenarios.

The predictions of surface runoff in the UYRB under the four future scenarios are shown in Figure 17. Table 7 provides the statistical characteristics and trends of surface runoff in the future. It can be seen that the mean annual surface runoff (MAR) values of the UYRB in the mid-term and long term are greater than those in the historical period, which indicates an increase in future surface runoff in the UYRB.

In the mid-term (2036–2065), SSP1-2.6 has the largest MAR of 467.22 mm, which is an increase of 12.09% compared with the historical period, followed by SSP3-7.0 at 453.75 mm (an increase of 8.86%), SSP2-4.5 at 450.79 mm (an increase of 8.15%), and SSP5-8.5 at 440.87 mm (an increase of 5.77%). Surface runoff tends to decrease under all four future scenarios. Surface runoff decreases significantly (at a 5% level) under SSP1-2.6, with a slope of −9.46 mm/decade. SSP5-8.5 has the largest slope of −11.06 mm/decade.

In the long term (2071–2100), the MAR values of the four future scenarios do not differ significantly from those in the mid-term (2036–2065). The MAR is the largest under SSP1-2.6 with 469.27 mm. Surface runoff under all four scenarios shows an increasing trend, which is the opposite of the mid-term. Surface runoff increased significantly (at a 5% level) under SSP1-2.6, with a trend slope of 7.99 mm/decade. SSP2-4.5 has the largest trend slope of 9.15 mm/decade.

**Table 7.** Projected mean annual surface runoff (MAR) change in different future periods in the UYRB.

	1985–2014			2036–2065			2071–2100		
	<b>MAR (mm)</b>	<i>Z<sub>MK</sub></i>	<b>Slope (mm/Decade)</b>	<b>MAR (mm)</b>	<i>Z<sub>MK</sub></i>	<b>Slope (mm/Decade)</b>	<b>MAR (mm)</b>	<i>Z<sub>MK</sub></i>	<b>Slope (mm/Decade)</b>
Historical period	416.82	−1.41	−14.43						
SSP1-2.6				467.22	−2.32	−9.46	469.27	1.97	7.99
SSP2-4.5				450.79	−0.46	−3.57	445.31	1.43	9.15
SSP3-7.0				453.75	−1.36	−6.71	453.80	0.32	2.35
SSP5-8.5				440.87	−1.32	−11.06	442.72	1.64	8.89

Note: The “**Bold**” represents a significant result at the 5% level. The “*italics*” represent the MMK values of time series with autocorrelation.

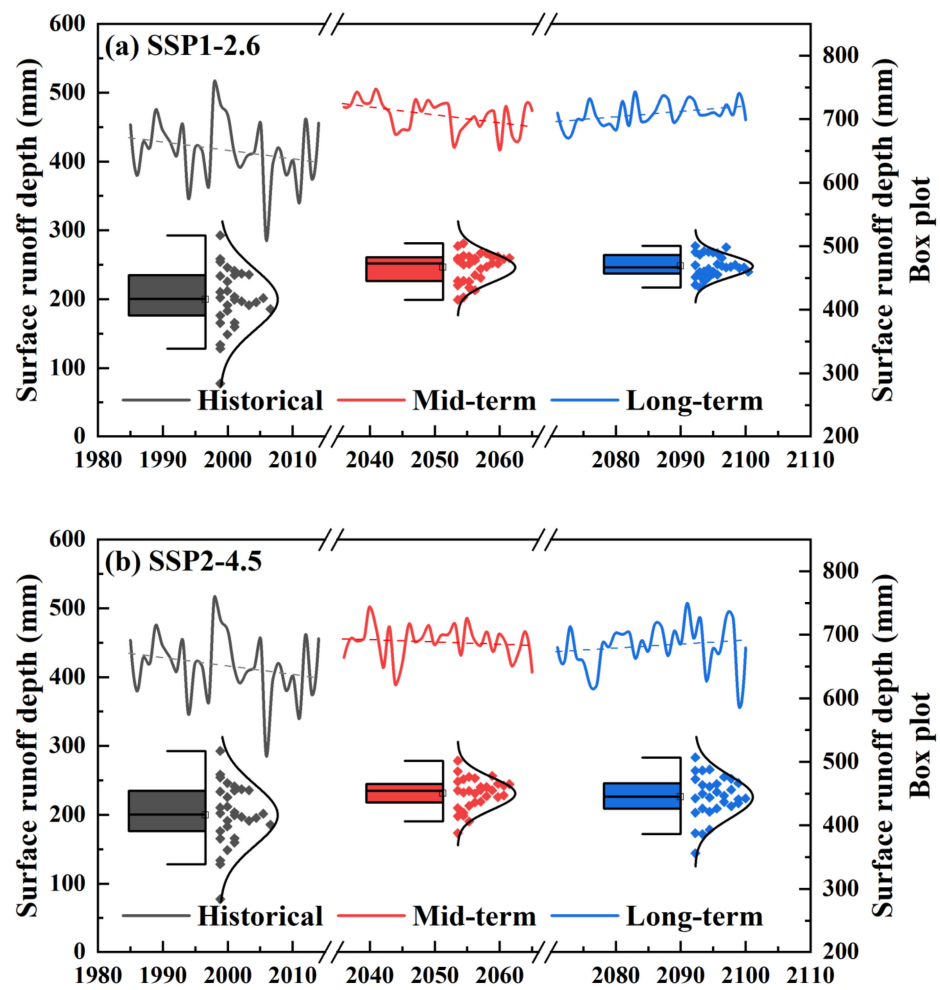


**Figure 17.** Cont.

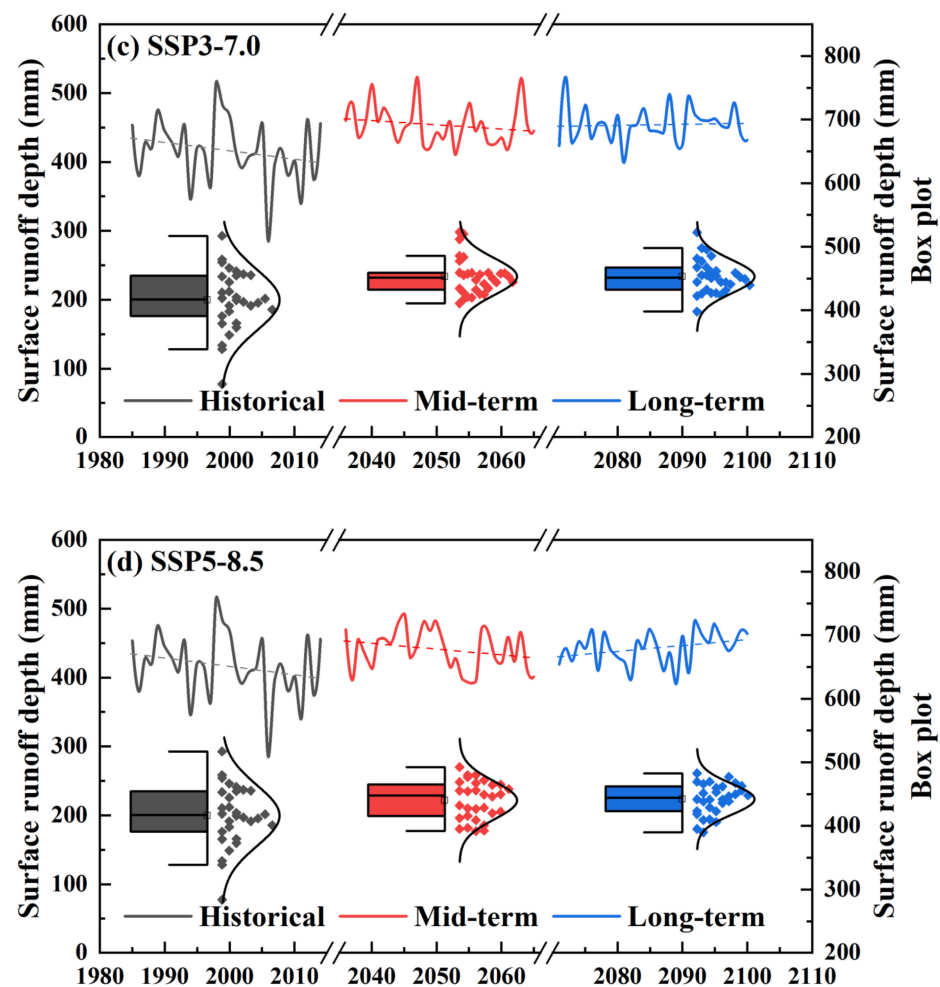


**Figure 17.** Surface runoff depth in the UYRB under the four future scenarios, (a) SSP1-2.6, (b) SSP2-4.5, (c) SSP3-7.0, and (d) SSP5-8.5.

## 4. Discussion and Limitations of the Study

### 4.1. Discussion

During the historical period (1985–2014), the climate in the UYRB exhibited a trend towards warming and humidification. Both annual precipitation and annual average temperature increased over time, with the warming and humidification trend being more pronounced in the northwest and central regions compared to the other areas. The increase in precipitation across the entire basin was not significant. Spatially, the areas showing an increasing trend in precipitation were mainly located in the northwest and in the Jialing River basin. The closer to the source of the Yangtze River, the greater the slope increase in annual precipitation. The temperature series in the whole UYRB showed a significant increasing trend. Spatially, the slope of temperature decreased from northwest to southeast, with the source area and central region of the UYRB experiencing a larger increase in temperature.

In the future period, the MAP and MAT values of the UYRB were shown to be greater than those in the historical period. The climate of the UYRB will experience warming and humidification in the future. The trend slopes of precipitation and temperature increase with increasing radiative forcing. These findings are consistent with the conclusions of the study conducted by Li et al. (2021), Zhu et al. (2021), and Wu et al. (2022) [2,43,73].

Our study reveals that the temporal and spatial variation patterns of precipitation and temperature under SSP1-2.6 in the UYRB are different from the other three scenarios. The precipitation series under SSP1-2.6 first decreases and then increases from the mid-

term (2036–2065) to the long term (2071–2100), while the temperature under SSP1-2.6 first increases and then decreases. Precipitation and temperature under the other three scenarios show increasing trends in both the mid-term (2036–2065) and long term (2071–2100). The reason for this is that SSP1-2.6 represents the sustainable development pathway with a low radiative forcing level. The SSP1-2.6 scenario involves sustainable development practices and proactive measures to mitigate climate change, resulting in lower fossil fuel consumption and greenhouse gas emissions compared to the other scenarios [74,75]. Another low radiative forcing scenario, SSP2-4.5, shows an overall increasing trend in precipitation and temperature. Comparatively, the high radiative forcing scenarios, SSP3-7.0 and SSP5-8.5, characterized by intensive social and economic development patterns with substantial fossil fuel consumption and greenhouse gas emissions, lead to significant increases in precipitation and temperature across all future periods. At the spatial scale, the mean annual precipitation and mean annual temperature in the UYRB under the four future scenarios exhibit similar spatial distribution patterns to the historical period. The upstream region generally experiences lower precipitation and temperatures compared to the downstream region, primarily due to variations in elevation and topography. At the same time, the warming and humidification of the climate are more pronounced in the high-altitude regions.

In the process of identifying key climatic factors affecting surface runoff, the results of the random forest regression model are more reasonable than those of the Spearman rank correlation test. This may be because the relationship between climatic factors and surface runoff is very complex, and traditional statistical analysis methods have weaker recognition and processing capabilities than machine learning algorithms for this complex relationship. According to the results of the random forest regression model, the surface runoff in the UYRB is mainly affected by annual precipitation,  $R \times 5\text{day}$ , and annual average temperature. The sum of the three factors' interpretation degree of surface runoff reaches 85%. Annual precipitation is the most important influencing factor of surface runoff, followed by  $R \times 5\text{day}$  and temperature. From the parameters of the multiple linear regression model, it can be seen that precipitation and  $R \times 5\text{day}$  are positively correlated with surface runoff, while temperature is negatively correlated with surface runoff. This is because precipitation is an important source of surface runoff, and changes in temperature affect evaporative conditions in the region. An increase in air temperature leads to stronger evaporation, which in turn increases the amount of surface runoff loss [76].

During the historical period (1985–2014), the surface runoff in the UYRB exhibited a decreasing trend [8,30]. The MAR values of the UYRB were higher than the historical period under all four scenarios, and the streamflow in the UYRB increased [11,46]. Compared with the historical period, the SSP1-2.6 scenario showed the highest increase in surface runoff, with an increase of 12.09% in the mid-term (2036–2065) and 12.58% in the long term (2071–2100). Surface runoff under all four scenarios showed a decreasing trend in the mid-term (2036–2065) and an increasing trend in the long term (2071–2100). Among the four scenarios, only the surface runoff trends under SSP1-2.6 were significant (at a 5% level) in both the mid-term and long term. This is due to the unique temporal and spatial variation patterns of climate under SSP1-2.6. In the mid-term (2036–2065), decreasing precipitation and increasing temperatures under SSP1-2.6 resulted in a significant (at a 5% level) decrease in surface runoff due to decreased recharge and increased loss of surface runoff. Similarly, when precipitation increased and temperature decreased in the long term (2071–2100), surface runoff increased significantly (at a 5% level).

The trends of surface runoff are not significant under SSP2-4.5, SSP3-7.0, or SSP5-8.5. This is due to the fact that precipitation and temperature act in opposite directions on surface runoff under these three scenarios. Under SSP2-4.5, SSP3-7.0, and SSP5-8.5, both precipitation and temperature increase in all future periods. However, the trends of surface runoff in two future periods are different. This indicates that the intensity of the influence of precipitation and temperature on surface runoff will change in different future periods. In the mid-term (2036–2065), the influence of temperature on surface runoff dominates,

causing surface runoff to decrease. In the long term (2071–2100), precipitation has a stronger influence on surface runoff than temperature.

#### 4.2. Limitations of This Study

It should be acknowledged that this study contains some limitations. First, in this study, the mean of a model ensemble is used as the future climate projection in the UYRB [77]. However, no further analysis was conducted on the uncertainty of the predicted results. This may lead to an incomplete analysis when discussing the impact of climate change on surface runoff [1].

Second, no physically based hydrologic models (e.g., SWAT) were used to predict future surface runoff in this study, but rather a data-driven climate–runoff prediction model was utilized. The reason for this is that building a reliable hydrologic model usually requires a large amount of observational data, including daily precipitation, daily maximum temperature, daily minimum temperature, runoff records, and some other spatial data [78]. In this study, the data we collected were daily precipitation, daily mean temperature, and annual runoff at the watershed outlet, and it is difficult to build a reliable hydrological model using these data, so a data-driven climate–runoff prediction model is a better choice. It must also be acknowledged that the climate–runoff prediction model developed in this paper has limited accuracy and can only be used to analyze surface runoff trends. This is because the model only considers climate change, and other factors that affect surface runoff, such as land use and human activities, are not considered.

### 5. Conclusions

This study analyzed the temporal and spatial patterns of precipitation and temperature in the upper Yangtze River basin (UYRB) during the historical period (1985–2014) and two future periods: mid-term (2036–2065) and long term (2071–2100). The key climatic factors influencing surface runoff were identified, and the surface runoff sequence under climate change conditions was predicted. The main conclusions are as follows:

- (1) During the historical period (1985–2014), the UYRB experienced warming and humidification trends, with both annual precipitation and temperature increasing over time. The warming and humidification trends were more pronounced in the northwestern and central regions.
- (2) Under SSP1-2.6, SSP2-4.5, SSP3-7.0, and SSP5-8.5, relative to those in the historical period (1985–2014), the mean annual precipitation (MAP) and mean annual average temperature (MAT) over the UYRB increase in the future. The MAP and MAT values increase more in the long term (2071–2100) than in the mid-term (2036–2065).
- (3) Under SSP2-4.5, SSP3-7.0, and SSP5-8.5, precipitation and temperature show increasing trends in both the mid-term (2036–2065) and long term (2071–2100). Under SSP1-2.6, the precipitation series first decreases and then increases from the mid-term (2036–2065) to the long term (2071–2100), while the temperature first increases and then decreases. The trend slopes of precipitation and temperature are minimized under SSP1-2.6. This indicates that the sustainable development pathway is conducive to reducing the impact of climate change in the UYRB.
- (4) At the spatial scale, the humid regions (annual precipitation > 800 mm) and high-temperature regions (annual temperature > 20 °C) in the future are projected to increase. Conversely, the semi-arid regions (annual precipitation between 200 mm and 400 mm) and cold regions (annual temperature below 0 °C) are expected to decrease. These changes are enhanced with increasing values of radiative forcing. The slopes of precipitation and temperature are greater in high-altitude regions than those in low-altitude regions.
- (5) The introduction of the random forest regression algorithm can effectively improve the credibility of the identification of key climatic factors influencing surface runoff. Apart from annual precipitation and annual average temperature, the key climatic factors influencing surface runoff also include the extreme climate indicator,  $R \times 5\text{day}$ . Precip-

itation and  $R \times 5\text{day}$  are positively correlated with surface runoff, and temperature is negatively correlated with surface runoff.

- (6) Under SSP1-2.6, SSP2-4.5, SSP3-7.0, and SSP5-8.5, the mean annual surface runoff (MAR) values in the UYRB are greater than those in the historical period in both the mid-term (2036–2065) and the long term (2071–2100). Surface runoff tends to decrease in the mid-term (2036–2065) due to temperature increases and to increase in the long term (2071–2100) due to precipitation increases. Under SSP1-2.6, the surface runoff increases significantly (at a 5% level), which means the risk of flood disaster in the future in the UYRB may increase under the scenario of lower radiative forcing.

**Funding:** This research received no external funding.

**Data Availability Statement:** The data presented in this study are available on request from the corresponding author due to privacy.

**Acknowledgments:** We would like to thank the National Meteorological Science Data Center (<http://data.cma.cn/>, accessed on 15 June 2023) for providing meteorological observation data. The NOAA Physical Sciences Laboratory (PSL) (<https://psl.noaa.gov>, accessed on 15 June 2023) provided NCEP/DOE Reanalysis II data. The Institute of Mountain Hazards and Environment, CAS provided the workplace.

**Conflicts of Interest:** The author declares no conflict of interest.

## Appendix A

**Table A1.** Information on meteorological stations used in this study.

Number	Station Name	Short Name	Code	Latitude (°N)	Longitude (°E)
1	Wudaoliang	WDL	52908	35.22	93.08
2	Anduo	AND	55294	32.35	91.10
3	Tuotuohe	TTH	56004	34.22	92.43
4	Zaduo	ZAD	56018	32.88	95.28
5	Qumalai	QML	56021	34.12	95.80
6	Yushu	YUS	56029	33.00	96.97
7	Qingshuihe	QSH	56034	33.80	97.13
8	Shiqu	SHQ	56038	32.98	98.10
9	Dari	DAR	56046	33.75	99.65
10	Jiuzhi	JZH	56067	33.43	101.48
11	Minxian	MNX	56093	34.43	104.02
12	Wudu	WUD	56096	33.40	104.92
13	Suoxian	SUX	56106	31.88	93.78
14	Changdu	CHD	56137	31.15	97.17
15	Dege	DEG	56144	31.80	98.58
16	Seda	SED	56152	32.28	100.33
17	Ma'erkang	MEK	56172	31.90	102.23
18	Xiaojin	XAJ	56178	31.00	102.35
19	Songpan	SNP	56182	32.67	103.60
20	Wenjiang	WEJ	56187	30.75	103.87
21	Mianyang	MAY	56196	31.45	104.73
22	Batang	BAT	56247	30.00	99.10
23	Xinlong	XNL	56251	30.93	100.32
24	Ya'an	YAN	56287	29.98	103.00

**Table A1.** *Cont.*

Number	Station Name	Short Name	Code	Latitude (°N)	Longitude (°E)
25	Zuogong	ZUG	56331	29.67	97.83
26	Daocheng	DAC	56357	29.05	100.30
27	Kangding	KAN	56374	30.05	101.97
28	Leshan	LSH	56386	29.57	103.75
29	Deqin	DEQ	56444	28.48	98.92
30	Jiulong	JUL	56462	29.00	101.50
31	Leibo	LEB	56485	28.27	103.58
32	Yibin	YBN	56492	28.80	104.60
33	Xichang	XIC	56571	27.90	102.27
34	Lijiang	LIJ	56651	26.85	100.22
35	Huili	HUL	56671	26.65	102.25
36	Weining	WEN	56691	26.87	104.28
37	Dali	DAL	56751	25.70	100.18
38	Zhanyi	ZHY	56786	25.58	103.83
39	Maiji	MAJ	57014	34.57	105.87
40	Hanzhong	HAZ	57127	33.07	107.03
41	Wanyuan	WAY	57237	32.07	108.03
42	Fangxian	FAX	57259	32.03	110.77
43	Langzhong	LZH	57306	31.58	105.98
44	Daxian	DXN	57328	31.20	107.50
45	Zhenping	ZHP	57343	31.90	109.53
46	Badong	BAD	57355	31.03	110.37
47	Wanzhou	WAZ	57432	30.77	108.40
48	Lichuan	LCH	57439	30.28	108.93
49	Yichang	YIC	57461	30.73	111.37
50	Dongxingqu	DON	57503	29.62	105.12
51	Hechuan	HEC	57512	29.97	106.27
52	Fengdu	FED	57523	29.85	107.73
53	Xuyong	XYA	57608	28.17	105.43
54	Qijiang	QIJ	57612	29.00	106.65
55	Youyang	YOU	57633	28.82	108.77
56	Renhuai	REH	57710	27.80	106.40
57	Guiyang	GUI	57816	26.58	106.73
58	Kunming	KUN	56778	25.00	102.65

**Table A2.** The MK/MMK test (at 5% level) results and trend slope of annual mean precipitation and temperature over the UYRB during 1985–2014. The “\*” indicates passing the 5% significance level. The *italics* represent the MMK values of time series with autocorrelation. Positive/negative  $Z_{MK}$  values indicate increasing/decreasing trend.

Station	Annual Mean Precipitation		Annual Mean Temperature	
	$Z_{MK}$	Slope (mm/Decade)	$Z_{MK}$	Slope (°C/Decade)
AND	1.36	21.79	4.14 *	0.46
SUX	2.00 *	43.77	3.82 *	0.50

Table A2. Cont.

Station	Annual Mean Precipitation		Annual Mean Temperature	
	Z <sub>MK</sub>	Slope (mm/Decade)	Z <sub>MK</sub>	Slope (°C/Decade)
TTH	3.21 *	53.45	4.57 *	0.72
WDL	3.07 *	38.58	4.17 *	0.54
YUS	0.89	21.50	3.46 *	0.50
ZAD	0.71	9.20	4.50 *	0.58
QML	1.93	35.84	5.17 *	0.70
BAT	−1.00	−25.89	3.75 *	0.46
DEQ	−0.11	−7.29	4.03 *	0.49
ZUG	0.16	1.50	3.75 *	0.39
CHD	−1.30	−29.30	3.43 *	0.35
DEG	−0.29	−7.40	3.28 *	0.30
SHQ	0.87	16.27	3.71 *	0.54
DAR	2.00 *	36.36	4.28 *	0.54
QSH	1.57	30.67	4.71 *	0.66
KUN	−0.68	−42.82	4.03 *	0.61
DAL	−1.46	−63.44	4.07 *	0.45
HUL	−2.43 *	−101.83	3.64 *	0.38
LIJ	−1.64	−49.71	3.28 *	0.43
XIC	−0.75	−38.62	3.25 *	0.37
DAC	−0.21	−4.00	4.07 *	0.45
JUL	−0.29	−6.59	3.14 *	0.28
KAN	−1.02	−19.54	2.71 *	0.29
JZH	0.70	16.28	4.25 *	0.47
MEK	0.39	7.50	3.46 *	0.35
SED	0.39	7.14	3.96 *	0.38
XAJ	−0.66	−8.18	2.39 *	0.30
XNL	−0.07	−4.44	3.32 *	0.30
WEN	0.39	20.80	3.53 *	0.44
ZHY	−2.18 *	−90.75	3.71 *	0.43
DON	0.68	87.94	0.32	0.06
LSH	−0.46	−13.18	3.18 *	0.38
LEB	−0.16	−10.50	4.42 *	0.99
XYA	−0.32	−11.78	2.85 *	0.28
YAN	−1.28	−78.91	2.07 *	0.23
YBN	−1.25	−60.67	3.75 *	0.41
MAY	0.93	36.00	3.21 *	0.47
SNP	1.14	17.36	3.14 *	0.33
WEJ	0.04	6.54	2.96 *	0.35
WUD	0.36	5.59	3.03 *	0.37
MNX	0.54	12.07	3.96 *	0.42

Table A2. Cont.

Station	Annual Mean Precipitation		Annual Mean Temperature	
	Z <sub>MK</sub>	Slope (mm/Decade)	Z <sub>MK</sub>	Slope (°C/Decade)
GUI	−0.21	−11.26	−3.68 *	−0.42
REH	−1.75	−47.71	2.28 *	0.20
FED	−0.36	−11.67	3.14 *	0.35
HEC	0.21	11.60	3.10 *	0.32
QIJ	0.75	29.88	0.86	0.11
DXN	1.28	61.00	3.21 *	0.29
HAZ	1.50	73.56	5.10 *	0.54
LZH	0.96	45.05	3.03 *	0.32
WAY	1.28	59.00	2.50 *	0.26
MAJ	0.57	14.53	3.14 *	0.30
LCH	−1.61	−43.53	3.07 *	0.29
YOU	0.71	48.20	1.89	0.21
BAD	0.61	22.79	1.21	0.11
FAX	−0.29	−4.92	2.32 *	0.21
WAZ	−0.18	−4.75	3.57 *	0.38
ZHP	0.64	27.67	2.60 *	0.26
YIC	0.04	1.72	2.28 *	0.29
UYRB	0.82	10.44	4.14 *	0.42

Table A3. The MK/MMK test (at 5% level) results and trend slope (mm/decade) of annual mean precipitation over the UYRB during 2036–2065. The **bold** indicates passing the 5% significance level. The *italics* represent the MMK values of time series with autocorrelation. Positive/negative Z<sub>MK</sub> values indicate increasing/decreasing trend.

Station	Mid-Term (2036–2065)								Long-Term (2071–2100)							
	SSP1-2.6		SSP2-4.5		SSP3-7.0		SSP5-8.5		SSP1-2.6		SSP2-4.5		SSP3-7.0		SSP5-8.5	
	Z <sub>MK</sub>	Slope	Z <sub>MK</sub>	Slope	Z <sub>MK</sub>	Slope	Z <sub>MK</sub>	Slope	Z <sub>MK</sub>	Slope	Z <sub>MK</sub>	Slope	Z <sub>MK</sub>	Slope	Z <sub>MK</sub>	Slope
AND	0.29	4.84	<b>3.14</b>	37.35	3.32	59.75	<b>3.96</b>	70.65	−0.86	−12.62	0.29	2.29	<b>3.39</b>	53.08	<b>3.32</b>	67.81
SUX	−1.53	−12.99	−2.82	−24.11	−3.60	−28.32	−3.00	−24.74	1.11	6.51	−1.50	−9.42	−3.25	−22.81	−3.78	−32.70
TTH	0.93	5.42	<b>4.03</b>	22.71	<b>3.64</b>	32.34	<b>4.82</b>	40.05	−0.18	−0.65	1.64	12.04	<b>3.57</b>	41.51	5.25	63.75
WDL	0.57	4.11	3.07	23.52	<b>3.14</b>	31.59	<b>3.82</b>	40.34	−0.21	−2.60	0.07	0.44	<b>3.32</b>	40.94	<b>4.89</b>	54.93
YUS	−0.18	−0.70	−2.68	−12.29	−4.03	−17.58	−4.82	−24.95	<b>2.03</b>	6.22	0.07	0.11	−4.57	−23.41	−6.03	−29.33
ZAD	−0.89	−5.15	−0.29	−2.54	−0.32	−3.80	−0.11	−1.04	0.54	2.32	−1.21	−10.75	1.07	9.37	<b>2.96</b>	24.82
QML	1.11	8.41	<b>2.75</b>	22.50	<b>3.39</b>	30.21	<b>4.21</b>	40.57	1.03	6.49	0.36	2.10	<b>3.21</b>	30.67	<b>5.71</b>	66.05
BAT	−0.43	−5.04	1.36	13.69	<b>2.32</b>	22.27	1.57	16.91	1.18	7.20	1.32	10.99	<b>3.28</b>	35.22	<b>3.85</b>	45.67
DEQ	−1.25	−10.67	1.64	15.31	0.46	7.32	1.68	12.38	0.61	6.67	1.39	17.50	<b>2.75</b>	29.92	<b>3.21</b>	39.17
ZUG	−0.75	−5.57	1.03	11.00	1.53	12.99	1.03	10.61	1.36	13.13	1.78	16.72	<b>3.07</b>	33.45	<b>3.10</b>	36.03
CHD	−0.43	−3.32	0.32	2.45	<b>2.57</b>	23.98	1.93	17.36	0.46	3.58	−0.46	−4.92	<b>2.75</b>	31.16	<b>3.82</b>	44.09
DEG	0.50	2.93	<b>3.07</b>	19.43	<b>4.00</b>	39.73	<b>4.17</b>	34.61	0.46	4.31	−0.46	−2.43	<b>4.25</b>	38.58	5.25	74.61

Table A3. Cont.

Station	Mid-Term (2036–2065)								Long-Term (2071–2100)							
	SSP1-2.6		SSP2-4.5		SSP3-7.0		SSP5-8.5		SSP1-2.6		SSP2-4.5		SSP3-7.0		SSP5-8.5	
	Z <sub>MK</sub>	Slope	Z <sub>MK</sub>	Slope	Z <sub>MK</sub>	Slope	Z <sub>MK</sub>	Slope	Z <sub>MK</sub>	Slope	Z <sub>MK</sub>	Slope	Z <sub>MK</sub>	Slope	Z <sub>MK</sub>	Slope
SHQ	0.75	4.67	1.61	10.56	2.32	19.23	<b>1.96</b>	17.68	1.11	7.22	−0.93	−7.91	<b>2.82</b>	23.58	<b>4.89</b>	54.08
DAR	1.50	10.52	2.32	19.46	<b>2.96</b>	21.85	<b>3.64</b>	36.62	1.89	13.95	−0.11	−1.61	<b>3.35</b>	33.61	<b>5.03</b>	62.98
QSH	1.21	8.56	<b>2.46</b>	21.41	<b>2.85</b>	22.50	<b>3.28</b>	31.43	<b>2.03</b>	13.79	−0.43	−2.11	<b>3.60</b>	34.30	<b>5.14</b>	61.20
KUN	−1.18	−17.59	0.04	1.04	− <b>2.11</b>	−45.93	− <b>3.18</b>	−62.66	0.54	9.27	1.82	27.93	− <b>2.11</b>	−37.41	− <b>2.53</b>	−60.56
DAL	−2.25	−34.73	0.46	4.73	−1.21	−26.09	− <b>2.57</b>	−47.59	−0.18	−3.72	0.00	0.00	0.71	9.56	−0.64	−18.50
HUL	−0.39	−5.44	<b>2.71</b>	65.10	1.96	41.76	1.14	27.39	1.18	18.76	<b>2.36</b>	58.17	<b>3.50</b>	68.20	3.78	95.88
LIJ	−1.96	−24.09	1.68	31.46	1.07	26.32	0.93	15.79	−0.43	−6.01	1.39	27.02	<b>3.60</b>	61.62	<b>2.93</b>	65.46
XIC	0.00	−0.74	<b>2.00</b>	39.20	1.68	33.70	1.39	28.81	0.79	13.87	<b>2.28</b>	45.17	<b>2.96</b>	54.39	<b>3.82</b>	85.84
DAC	−1.46	−12.68	−0.39	−4.85	−0.14	−2.26	−0.75	−11.91	1.57	14.23	0.32	3.43	<b>2.11</b>	23.47	<b>2.50</b>	29.83
JUL	−0.79	−13.95	<b>2.50</b>	32.84	<b>3.53</b>	69.00	<b>2.96</b>	48.83	1.03	10.84	1.53	23.85	<b>4.71</b>	88.31	<b>5.60</b>	106.68
KAN	0.57	5.23	0.96	9.39	1.75	15.98	0.82	10.22	1.43	19.08	0.93	9.12	0.93	6.94	<b>2.32</b>	25.59
JZH	0.86	6.54	0.32	5.57	<b>3.64</b>	53.58	<b>4.32</b>	51.90	0.25	1.97	1.11	9.37	<b>4.50</b>	50.48	<b>5.71</b>	93.95
MEK	0.68	7.27	1.50	14.00	<b>4.10</b>	62.85	<b>4.46</b>	59.65	0.29	3.50	0.89	9.71	<b>5.07</b>	65.07	<b>5.64</b>	103.15
SED	0.25	1.91	−1.07	−8.45	<b>2.28</b>	24.56	1.93	14.62	1.64	11.11	0.25	3.84	<b>2.75</b>	27.62	<b>4.50</b>	52.85
XAJ	1.43	10.63	0.14	1.90	<b>4.14</b>	42.48	<b>4.28</b>	44.46	0.75	3.70	0.71	7.28	<b>4.03</b>	31.62	<b>5.78</b>	60.96
XNL	−0.36	−3.79	−1.39	−10.22	−0.71	−7.29	−1.39	−16.33	<b>2.21</b>	18.08	−0.64	−8.30	−0.04	−1.34	<b>2.46</b>	16.05
WEN	−0.93	−10.99	0.50	8.60	−1.14	−17.58	−1.82	−25.83	0.00	−0.59	0.61	11.55	1.50	18.93	0.07	1.68
ZHY	−0.46	−3.72	1.39	24.90	−0.25	−3.93	−0.07	−1.74	−0.07	−0.10	0.93	18.34	1.75	33.48	1.71	30.29
DON	− <b>2.39</b>	−34.74	1.32	17.65	1.36	24.84	1.46	17.99	0.82	7.44	<b>2.07</b>	34.65	1.71	29.06	<b>3.18</b>	46.25
LSH	−1.93	−36.63	−0.71	−12.99	−1.78	−36.42	−1.11	−25.73	1.50	21.65	0.57	12.10	0.68	17.99	0.04	0.81
LEB	−1.53	−17.53	0.46	4.10	−0.75	−9.47	−0.64	−5.04	−0.07	−1.03	0.21	4.67	1.18	18.70	1.46	18.79
XYA	−0.93	−7.95	0.64	5.38	−0.32	−2.80	1.14	11.04	0.32	1.59	0.93	6.69	1.14	15.66	<b>2.71</b>	23.28
YAN	−1.14	−26.34	−1.03	−31.06	−1.32	−31.36	−1.46	−34.33	<b>2.21</b>	34.15	−0.04	−2.20	0.61	13.91	−0.36	−3.06
YBN	−1.75	−29.15	−1.03	−19.09	− <b>2.32</b>	−42.93	− <b>2.18</b>	−36.57	<b>2.03</b>	26.99	1.21	22.49	−0.86	−11.88	−0.86	−9.64
MAY	−1.53	−20.87	−1.50	−25.77	0.68	8.49	−0.21	−3.17	1.32	16.80	1.75	23.47	0.46	12.99	<b>2.46</b>	35.47
SNP	−0.07	−0.64	0.57	4.60	<b>2.85</b>	22.80	<b>3.78</b>	30.26	1.96	15.53	1.89	12.70	<b>3.39</b>	32.90	<b>5.64</b>	56.37
WEJ	−0.96	−18.09	−1.89	−28.12	0.50	7.37	−1.14	−18.89	1.78	19.24	1.39	17.40	−0.11	−1.31	0.29	3.31
WUD	−1.36	−10.61	−1.25	−7.56	1.32	8.79	1.32	6.56	1.32	12.06	<b>2.07</b>	14.37	0.71	8.65	<b>2.68</b>	18.19
MNX	0.25	1.12	−0.39	−4.70	1.46	21.27	1.39	10.93	−0.25	−3.33	1.93	17.49	1.61	16.46	<b>3.78</b>	40.58
GUI	1.21	13.21	1.46	22.30	1.21	19.08	0.93	13.41	−0.68	−7.39	0.36	5.79	0.61	8.19	<b>2.57</b>	48.60
REH	0.86	10.19	<b>2.00</b>	24.06	1.71	20.38	1.21	13.29	−1.82	−19.02	−0.39	−7.28	1.18	13.55	<b>2.25</b>	45.01
FED	−0.36	−3.49	<b>2.46</b>	23.59	<b>3.00</b>	19.47	<b>2.21</b>	24.49	−0.46	−5.40	1.28	17.43	1.46	18.88	<b>3.07</b>	38.67
HEC	−1.28	−25.06	0.21	2.88	0.29	5.26	0.18	0.95	−1.00	−13.67	0.61	11.82	−0.18	−3.88	1.75	43.06
QIJ	− <b>2.14</b>	−23.68	1.50	18.62	0.36	5.78	<b>2.60</b>	41.04	−0.79	−5.88	1.25	16.78	<b>2.25</b>	24.47	<b>4.03</b>	70.54
DXN	−0.89	−8.34	0.50	7.08	<b>2.57</b>	38.56	<b>2.28</b>	40.35	0.64	6.24	1.32	23.65	<b>3.21</b>	47.03	<b>5.14</b>	76.90
HAZ	−0.68	−8.65	0.07	2.25	1.50	20.49	0.93	20.73	0.71	10.52	1.61	27.82	1.03	20.94	<b>2.14</b>	34.38
LZH	−1.07	−17.83	−0.39	−6.81	1.14	18.12	1.32	20.96	1.50	18.50	<b>2.14</b>	41.28	1.28	36.48	<b>2.28</b>	42.70
WAY	−0.75	−15.93	0.11	3.58	<b>2.00</b>	34.60	1.64	37.31	0.93	14.31	1.82	46.71	1.00	22.58	<b>2.64</b>	61.00
MAJ	0.46	4.35	−0.18	−3.43	1.50	20.64	0.75	7.02	0.00	−0.57	1.68	22.02	1.28	21.22	<b>2.78</b>	33.00
LCH	−0.11	−0.52	1.93	38.13	<b>2.14</b>	32.81	1.89	36.42	−0.04	−1.80	0.18	2.53	1.36	17.61	<b>3.43</b>	100.78
YOU	0.89	12.01	1.21	26.38	0.68	11.83	0.57	9.44	−0.11	−1.18	0.71	15.84	0.07	0.22	<b>2.53</b>	56.77
BAD	−1.18	−10.60	1.43	17.07	1.46	23.08	<b>2.28</b>	38.00	0.46	3.07	1.25	18.48	<b>2.07</b>	35.42	<b>3.60</b>	59.35
FAX	−0.29	−2.41	1.00	12.64	1.86	20.81	<b>2.18</b>	32.25	−0.32	−2.31	0.75	12.08	<b>3.00</b>	41.28	<b>3.43</b>	53.46
WAZ	−1.03	−10.31	1.64	28.23	<b>2.21</b>	44.90	<b>2.93</b>	59.33	0.18	1.51	1.53	28.08	<b>3.18</b>	50.70	<b>4.57</b>	99.84
ZHP	−0.89	−8.12	0.89	12.53	1.32	19.73	1.86	38.40	0.68	9.17	1.11	22.32	<b>2.64</b>	53.75	<b>3.57</b>	79.28
YIC	0.32	3.87	1.03	16.33	0.93	22.52	1.50	26.25	1.61	30.17	1.00	20.85	<b>2.18</b>	41.49	<b>2.36</b>	53.35
UYRB	−0.89	−5.30	1.61	12.08	<b>2.18</b>	17.06	1.93	12.37	1.14	7.08	<b>2.00</b>	16.68	<b>3.43</b>	29.17	<b>4.67</b>	47.93

**Table A4.** The MK test results and trend slope (°C/decade) of annual mean temperature over the UYRB during 2015–2100. The **bold** indicates passing the 5% significance level. The *italics* represent the MMK values of time series with autocorrelation. Positive/negative  $Z_{MK}$  values indicate increasing/decreasing trend.

Station	Mid-Term (2036–2065)								Long-Term (2071–2100)							
	SSP1-2.6		SSP2-4.5		SSP3-7.0		SSP5-8.5		SSP1-2.6		SSP2-4.5		SSP3-7.0		SSP5-8.5	
	$Z_{MK}$	Slope	$Z_{MK}$	Slope	$Z_{MK}$	Slope	$Z_{MK}$	Slope	$Z_{MK}$	Slope	$Z_{MK}$	Slope	$Z_{MK}$	Slope	$Z_{MK}$	Slope
AND	1.46	0.11	<b>4.46</b>	0.30	<b>6.17</b>	0.66	<b>5.92</b>	0.68	−0.93	−0.06	<b>2.07</b>	0.09	<b>5.28</b>	0.54	<b>6.21</b>	0.78
SUX	<b>2.03</b>	0.12	<b>4.82</b>	0.29	<b>6.21</b>	0.61	<b>6.21</b>	0.61	−0.57	−0.03	<b>2.78</b>	0.09	<b>5.46</b>	0.53	<b>6.14</b>	0.71
TTH	<b>2.46</b>	0.12	<b>4.96</b>	0.29	<b>6.14</b>	0.57	<b>5.89</b>	0.53	−1.32	−0.05	<b>2.11</b>	0.07	<b>5.46</b>	0.51	<b>6.35</b>	0.69
WDL	<b>2.43</b>	0.16	<b>4.89</b>	0.33	<b>5.92</b>	0.61	<b>6.10</b>	0.60	−2.14	−0.08	<b>2.00</b>	0.08	<b>5.71</b>	0.57	<b>6.35</b>	0.72
YUS	<b>2.71</b>	0.18	<b>5.21</b>	0.32	<b>6.14</b>	0.58	<b>6.42</b>	0.58	−0.96	−0.05	<b>3.03</b>	0.10	<b>5.50</b>	0.53	<b>6.17</b>	0.70
ZAD	<b>2.93</b>	0.21	<b>5.39</b>	0.33	<b>5.89</b>	0.60	<b>6.39</b>	0.60	−1.21	−0.06	<b>2.89</b>	0.11	<b>5.46</b>	0.58	<b>6.10</b>	0.72
QML	<b>2.57</b>	0.16	<b>5.39</b>	0.31	<b>5.67</b>	0.55	<b>6.14</b>	0.52	−1.53	−0.06	<b>1.75</b>	0.07	<b>5.96</b>	0.51	<b>6.14</b>	0.61
BAT	<b>4.07</b>	0.17	<b>4.57</b>	0.24	<b>6.07</b>	0.42	<b>6.39</b>	0.44	0.61	0.02	<b>2.36</b>	0.08	<b>5.46</b>	0.43	<b>6.46</b>	0.56
DEQ	<b>3.35</b>	0.17	<b>5.14</b>	0.28	<b>6.28</b>	0.58	<b>6.53</b>	0.61	−1.32	−0.06	<b>4.17</b>	0.14	<b>6.10</b>	0.56	<b>6.60</b>	0.73
ZUG	<b>3.50</b>	0.18	<b>4.75</b>	0.27	<b>5.67</b>	0.52	<b>6.46</b>	0.58	−0.79	−0.04	<b>3.28</b>	0.14	<b>5.74</b>	0.55	<b>6.39</b>	0.68
CHD	<b>2.85</b>	0.19	<b>5.14</b>	0.33	<b>5.82</b>	0.53	<b>6.21</b>	0.55	−1.28	−0.07	<b>2.50</b>	0.09	<b>5.46</b>	0.51	<b>5.89</b>	0.67
DEG	<b>3.35</b>	0.18	<b>5.21</b>	0.29	<b>5.78</b>	0.50	<b>6.42</b>	0.51	−1.57	−0.07	<b>2.32</b>	0.08	<b>5.64</b>	0.47	<b>6.24</b>	0.62
SHQ	<b>3.18</b>	0.23	<b>5.28</b>	0.35	<b>5.99</b>	0.66	<b>6.46</b>	0.70	−0.96	−0.06	<b>3.35</b>	0.14	<b>5.53</b>	0.64	<b>6.46</b>	0.82
DAR	<b>3.57</b>	0.17	<b>5.39</b>	0.31	<b>5.92</b>	0.52	<b>6.42</b>	0.58	−1.25	−0.04	<b>2.25</b>	0.08	<b>6.07</b>	0.57	<b>6.35</b>	0.79
QSH	<b>3.89</b>	0.18	<b>5.25</b>	0.32	<b>5.85</b>	0.55	<b>6.21</b>	0.60	−1.39	−0.04	<b>2.07</b>	0.09	<b>6.21</b>	0.60	<b>6.39</b>	0.84
KUN	<b>3.10</b>	0.15	<b>4.35</b>	0.32	<b>4.39</b>	0.34	<b>6.03</b>	0.57	−0.11	0.00	<b>1.25</b>	0.08	<b>5.32</b>	0.46	<b>6.28</b>	0.66
DAL	<b>4.00</b>	0.15	<b>4.60</b>	0.23	<b>5.10</b>	0.33	<b>6.46</b>	0.48	−0.89	−0.03	<b>1.25</b>	0.05	<b>5.71</b>	0.38	<b>6.57</b>	0.55
HUL	<b>3.82</b>	0.16	<b>4.64</b>	0.27	<b>5.17</b>	0.41	<b>6.49</b>	0.56	−0.36	−0.02	<b>1.46</b>	0.06	<b>5.60</b>	0.43	<b>6.49</b>	0.65
LIJ	<b>4.00</b>	0.18	<b>4.42</b>	0.27	<b>5.28</b>	0.46	<b>6.49</b>	0.59	−0.54	−0.03	<b>2.07</b>	0.09	<b>5.71</b>	0.47	<b>6.49</b>	0.68
XIC	<b>2.85</b>	0.13	<b>4.03</b>	0.31	<b>4.78</b>	0.42	<b>6.07</b>	0.67	0.07	0.00	<b>1.61</b>	0.08	<b>5.17</b>	0.50	<b>6.28</b>	0.76
DAC	<b>3.71</b>	0.17	<b>4.96</b>	0.24	<b>6.10</b>	0.53	<b>6.60</b>	0.54	−0.89	−0.03	<b>3.71</b>	0.13	<b>6.10</b>	0.50	<b>6.60</b>	0.68
JUL	<b>3.64</b>	0.16	<b>4.92</b>	0.23	<b>5.92</b>	0.46	<b>6.64</b>	0.52	−1.07	−0.04	<b>3.14</b>	0.10	<b>5.96</b>	0.46	<b>6.60</b>	0.63
KAN	<b>3.25</b>	0.16	<b>4.39</b>	0.30	<b>5.99</b>	0.57	<b>6.03</b>	0.55	−1.46	−0.05	<b>3.28</b>	0.13	<b>5.74</b>	0.51	<b>6.53</b>	0.76
JZH	<b>3.35</b>	0.18	<b>4.78</b>	0.31	<b>5.99</b>	0.60	<b>6.24</b>	0.61	−1.82	−0.09	<b>2.60</b>	0.12	<b>5.92</b>	0.56	<b>6.49</b>	0.77
MEK	<b>3.75</b>	0.13	<b>4.60</b>	0.18	<b>5.53</b>	0.34	<b>6.07</b>	0.38	−1.53	−0.05	<b>3.03</b>	0.09	<b>6.03</b>	0.32	<b>6.64</b>	0.46
SED	<b>3.53</b>	0.19	<b>4.78</b>	0.28	<b>5.74</b>	0.54	<b>6.53</b>	0.58	−1.43	−0.04	<b>3.25</b>	0.10	<b>6.24</b>	0.55	<b>6.46</b>	0.76
XAJ	<b>2.82</b>	0.16	<b>5.07</b>	0.28	<b>6.21</b>	0.58	<b>6.32</b>	0.57	−1.86	−0.07	<b>2.85</b>	0.09	<b>6.03</b>	0.49	<b>6.49</b>	0.72
XNL	<b>3.18</b>	0.16	<b>4.92</b>	0.25	<b>5.89</b>	0.47	<b>6.60</b>	0.51	−1.89	−0.04	<b>3.35</b>	0.08	<b>5.99</b>	0.44	<b>6.35</b>	0.63
WEN	<b>2.50</b>	0.12	<b>4.07</b>	0.27	<b>4.82</b>	0.47	<b>5.92</b>	0.59	0.07	0.01	<b>2.25</b>	0.16	<b>5.10</b>	0.49	<b>6.49</b>	0.73
ZHY	<b>2.46</b>	0.13	<b>4.17</b>	0.25	<b>4.78</b>	0.35	<b>5.85</b>	0.53	−0.39	−0.03	<b>2.00</b>	0.11	<b>5.10</b>	0.42	<b>6.39</b>	0.63
DON	<b>3.03</b>	0.14	<b>4.96</b>	0.27	<b>5.82</b>	0.42	<b>5.85</b>	0.45	−2.32	−0.07	0.96	0.05	<b>5.96</b>	0.40	<b>6.49</b>	0.59
LSH	<b>3.00</b>	0.14	<b>5.00</b>	0.25	<b>5.78</b>	0.40	<b>6.07</b>	0.42	−1.96	−0.07	1.46	0.05	<b>5.74</b>	0.36	<b>6.60</b>	0.57
LEB	<b>3.21</b>	0.16	<b>5.03</b>	0.29	<b>5.74</b>	0.50	<b>6.14</b>	0.54	−1.39	−0.07	<b>2.32</b>	0.11	<b>5.96</b>	0.46	<b>6.74</b>	0.70
XYA	<b>3.25</b>	0.16	<b>4.75</b>	0.28	<b>5.82</b>	0.48	<b>6.03</b>	0.52	−1.86	−0.06	1.86	0.09	<b>5.74</b>	0.44	<b>6.64</b>	0.68
YAN	<b>2.68</b>	0.13	<b>4.85</b>	0.25	<b>5.89</b>	0.41	<b>5.85</b>	0.42	−1.82	−0.06	1.86	0.06	<b>5.64</b>	0.35	<b>6.64</b>	0.56
YBN	<b>3.10</b>	0.15	<b>4.92</b>	0.27	<b>5.82</b>	0.42	<b>5.92</b>	0.47	−2.36	−0.07	1.46	0.06	<b>5.74</b>	0.41	<b>6.60</b>	0.61
MAY	<b>3.43</b>	0.15	<b>5.03</b>	0.29	<b>6.14</b>	0.48	<b>6.39</b>	0.48	−2.39	−0.08	1.61	0.07	<b>5.92</b>	0.41	<b>6.74</b>	0.62
SNP	<b>3.18</b>	0.16	<b>4.75</b>	0.27	<b>6.32</b>	0.52	<b>6.39</b>	0.54	−1.96	−0.06	<b>3.10</b>	0.13	<b>6.21</b>	0.48	<b>6.67</b>	0.68
WEJ	<b>3.28</b>	0.15	<b>4.89</b>	0.27	<b>6.28</b>	0.47	<b>6.35</b>	0.48	−2.32	−0.07	1.64	0.08	<b>5.89</b>	0.41	<b>6.78</b>	0.60
WUD	<b>3.28</b>	0.17	<b>4.92</b>	0.29	<b>5.89</b>	0.47	<b>6.17</b>	0.51	−2.03	−0.08	0.79	0.05	<b>5.78</b>	0.43	<b>6.53</b>	0.64
MNX	<b>3.14</b>	0.16	<b>5.00</b>	0.27	<b>6.21</b>	0.52	<b>6.46</b>	0.52	−1.75	−0.04	<b>2.28</b>	0.08	<b>5.89</b>	0.46	<b>6.64</b>	0.66
GUI	1.64	0.07	<b>4.46</b>	0.26	<b>5.10</b>	0.37	<b>5.78</b>	0.49	0.00	0.00	<b>2.07</b>	0.16	<b>5.46</b>	0.42	<b>6.14</b>	0.62
REH	<b>2.64</b>	0.15	<b>4.60</b>	0.38	<b>5.74</b>	0.61	<b>6.53</b>	0.73	−0.71	−0.03	<b>2.18</b>	0.17	<b>5.99</b>	0.64	<b>6.49</b>	0.93
FED	<b>3.14</b>	0.14	<b>4.85</b>	0.27	<b>5.85</b>	0.45	<b>5.96</b>	0.51	−1.07	−0.04	1.82	0.09	<b>5.89</b>	0.44	<b>6.57</b>	0.65
HEC	<b>3.35</b>	0.14	<b>4.53</b>	0.25	<b>5.74</b>	0.42	<b>5.85</b>	0.46	−0.54	−0.02	1.32	0.06	<b>5.74</b>	0.40	<b>6.17</b>	0.59

Table A4. Cont.

Station	Mid-Term (2036–2065)								Long-Term (2071–2100)							
	SSP1-2.6		SSP2-4.5		SSP3-7.0		SSP5-8.5		SSP1-2.6		SSP2-4.5		SSP3-7.0		SSP5-8.5	
	Z <sub>MK</sub>	Slope	Z <sub>MK</sub>	Slope	Z <sub>MK</sub>	Slope	Z <sub>MK</sub>	Slope	Z <sub>MK</sub>	Slope	Z <sub>MK</sub>	Slope	Z <sub>MK</sub>	Slope	Z <sub>MK</sub>	Slope
QIJ	3.32	0.16	4.82	0.29	5.64	0.50	6.14	0.54	−1.14	−0.05	1.89	0.11	5.92	0.49	6.39	0.69
DXN	3.71	0.17	5.32	0.30	6.17	0.52	6.21	0.54	−1.93	−0.07	1.78	0.08	6.03	0.45	6.49	0.70
HAZ	3.57	0.17	4.82	0.27	5.85	0.43	5.92	0.46	−2.18	−0.07	0.11	0.01	5.60	0.37	6.21	0.60
LZH	3.57	0.16	5.03	0.27	5.96	0.46	6.10	0.49	−2.57	−0.07	1.14	0.04	5.60	0.39	6.42	0.62
WAY	3.32	0.16	5.00	0.27	5.92	0.49	6.14	0.53	−2.21	−0.07	1.39	0.07	5.78	0.43	6.46	0.68
MAJ	3.35	0.16	4.46	0.28	5.85	0.49	6.24	0.51	−2.25	−0.07	0.57	0.02	5.35	0.42	6.17	0.63
LCH	2.57	0.12	4.82	0.29	6.10	0.46	6.28	0.52	−1.11	−0.05	2.46	0.12	6.39	0.45	6.42	0.64
YOU	2.36	0.12	4.78	0.29	6.03	0.49	6.53	0.53	−0.64	−0.02	2.57	0.14	6.32	0.48	6.42	0.70
BAD	3.21	0.17	4.92	0.29	6.24	0.55	6.03	0.57	−1.89	−0.07	1.39	0.08	6.17	0.49	6.32	0.69
FAX	3.43	0.16	5.07	0.29	6.17	0.52	5.99	0.54	−1.50	−0.06	0.96	0.06	6.03	0.47	6.49	0.69
WAZ	3.43	0.15	5.28	0.27	6.24	0.47	6.42	0.49	−1.89	−0.05	1.82	0.07	6.46	0.43	6.60	0.62
ZHP	3.10	0.17	4.64	0.31	6.42	0.56	6.17	0.59	−1.78	−0.06	1.96	0.10	6.07	0.51	6.46	0.77
YIC	2.43	0.13	4.39	0.32	5.57	0.54	5.78	0.55	−1.71	−0.07	1.89	0.12	5.78	0.51	6.35	0.71
UYRB	3.71	0.16	5.39	0.29	6.07	0.47	6.60	0.54	−1.75	−0.05	2.82	0.10	6.53	0.45	6.64	0.67

## References

- Yonaba, R.; Mounirou, L.A.; Tazen, F.; Koïta, M.; Biaou, A.C.; Zouré, C.O.; Queloz, P.; Karambiri, H.; Yacouba, H. Future climate or land use? Attribution of changes in surface runoff in a typical Sahelian landscape. *Comptes Rendus. Géoscience* **2023**, *335*, 1–28. [\[CrossRef\]](#)
- Li, Y.; Yan, D.; Peng, H.; Xiao, S. Evaluation of precipitation in CMIP6 over the Yangtze River Basin. *Atmos. Res.* **2021**, *253*, 105406. [\[CrossRef\]](#)
- Gou, J.J.; Miao, C.Y.; Duan, Q.Y.; Tang, Q.H.; Di, Z.H.; Liao, W.H.; Wu, J.W.; Zhou, R. Sensitivity Analysis-Based Automatic Parameter Calibration of the VIC Model for Streamflow Simulations Over China. *Water Resour. Res.* **2020**, *56*, e2019WR025968. [\[CrossRef\]](#)
- IPCC. Summary for policymakers. Global warming of 1.5 °C. In *An IPCC Special Report on the Impacts of Global Warming of 1.5 °C above Pre-Industrial Levels and Related Global Greenhouse Gas Emission Pathways*; World Meteorological Organization: Geneva, Switzerland, 2018; p. 32.
- Diffenbaugh, N.S.; Singh, D.; Mankin, J.S.; Horton, D.E.; Swain, D.L.; Touma, D.; Charland, A.; Liu, Y.J.; Haugen, M.; Tsiang, M.; et al. Quantifying the influence of global warming on unprecedented extreme climate events. *Proc. Natl. Acad. Sci. USA* **2017**, *114*, 4881–4886. [\[CrossRef\]](#) [\[PubMed\]](#)
- Trenberth, K.E.; Fasullo, J.T.; Shepherd, T.G. Attribution of climate extreme events. *Nat. Clim. Change* **2015**, *5*, 725–730. [\[CrossRef\]](#)
- Chen, J.; Gao, C.; Zeng, X.; Xiong, M.; Wang, Y.; Jing, C.; Krysanova, V.; Huang, J.; Zhao, N.; Su, B. Assessing changes of river discharge under global warming of 1.5 °C and 2 °C in the upper reaches of the Yangtze River Basin: Approach by using multiple-GCMs and hydrological models. *Quat. Int.* **2017**, *453*, 63–73. [\[CrossRef\]](#)
- Yang, R.; Xing, B. Spatio-Temporal Variability in Hydroclimate over the Upper Yangtze River Basin, China. *Atmosphere* **2022**, *13*, 317. [\[CrossRef\]](#)
- Seddon, A.W.R.; Macias-Fauria, M.; Long, P.R.; Benz, D.; Willis, K.J. Sensitivity of global terrestrial ecosystems to climate variability. *Nature* **2016**, *531*, 229–232. [\[CrossRef\]](#)
- Frame, D.J.; Rosier, S.M.; Noy, I.; Harrington, L.J.; Carey-Smith, T.; Sparrow, S.N.; Stone, D.A.; Dean, S.M. Climate change attribution and the economic costs of extreme weather events: A study on damages from extreme rainfall and drought. *Clim. Change* **2020**, *162*, 781–797. [\[CrossRef\]](#)
- Zhang, C.; Sun, F.; Sharma, S.; Zeng, P.; Mejia, A.; Lyu, Y.P.; Gao, J.; Zhou, R.; Che, Y. Projecting multi-attribute flood regime changes for the Yangtze River basin. *J. Hydrol.* **2023**, *617*, 128846. [\[CrossRef\]](#)
- Wu, L.; Wang, S.; Bai, X.; Chen, F.; Li, C.; Ran, C.; Zhang, S. Identifying the Multi-Scale Influences of Climate Factors on Runoff Changes in a Typical Karst Watershed Using Wavelet Analysis. *Land* **2022**, *11*, 1284. [\[CrossRef\]](#)
- Burns, D.A.; Klaus, J.; McHale, M.R. Recent climate trends and implications for water resources in the Catskill Mountain region, New York, USA. *J. Hydrol.* **2007**, *336*, 155–170. [\[CrossRef\]](#)
- Li, Z.; Xu, X.; Yu, B.; Xu, C.; Liu, M.; Wang, K. Quantifying the impacts of climate and human activities on water and sediment discharge in a karst region of southwest China. *J. Hydrol.* **2016**, *542*, 836–849. [\[CrossRef\]](#)
- Okafor, G.; Jimoh, O.D.; Larbi, K.I. Detecting Changes in Hydro-Climatic Variables during the Last Four Decades (1975–2014) on Downstream Kaduna River Catchment, Nigeria. *Appl. Categ. Struct.* **2017**, *07*, 161–175. [\[CrossRef\]](#)

16. Wu, L.; Chen, D.; Yang, D.; Luo, G.; Wang, J.; Chen, F. Response of Runoff Change to Extreme Climate Evolution in a Typical Watershed of Karst Trough Valley, SW China. *Atmosphere* **2023**, *14*, 927. [CrossRef]
17. Yang, Y.N.; Xu, C.C.; Yang, Y.H.; Hao, X.M.; Shen, Y.P. Hydrology and Water Resources Variation and Its Responses to Regional Climate Change in Xinjiang. *Acta Geogr. Sin.* **2009**, *64*, 1331–1341. [CrossRef]
18. Labat, D.; Godd ris, Y.; Probst, J.L.; Guyot, J.L. Evidence for global runoff increase related to climate warming. *Adv. Water Resour.* **2004**, *27*, 631–642. [CrossRef]
19. Qian, J.; Zhou, B.T. Changes of weather and climate extremes in the IPCC AR6. *Adv. Clim. Change Res.* **2021**, *17*, 713–718.
20. IPCC. Climate Change 2021: The Physical Science Basis. 2021. Available online: [https://www.ipcc.ch/report/ar6/wg1/downloads/report/IPCC\\_AR6\\_WGI\\_Full\\_Report.pdf](https://www.ipcc.ch/report/ar6/wg1/downloads/report/IPCC_AR6_WGI_Full_Report.pdf) (accessed on 15 June 2023).
21. Min, R.; Gu, X.; Guan, Y.; Zhang, X. Increasing likelihood of global compound hot-dry extremes from temperature and runoff during the past 120 years. *J. Hydrol.* **2023**, *621*, 129553. [CrossRef]
22. Gray, L.C.; Zhao, L.; Stillwell, A.S. Impacts of climate change on global total and urban runoff. *J. Hydrol.* **2023**, *620*, 129352. [CrossRef]
23. Nayak, P.C.; Sudheer, K.P.; Jain, S.K. Rainfall-runoff modeling through hybrid intelligent system. *Water Resour. Res.* **2007**, *43*, W07415. [CrossRef]
24. Wang, Y.; Guo, S.; Chen, H.; Zhou, Y. Comparative study of monthly inflow prediction methods for the Three Gorges Reservoir. *Stoch. Environ. Res. Risk Assess.* **2014**, *28*, 555–570. [CrossRef]
25. Li, W.; Yang, M.; Liang, Z.; Zhu, Y.; Mao, W.; Shi, J.; Chen, Y.-x. Assessment for surface water quality in Lake Taihu Tiaoxi River Basin China based on support vector machine. *Stoch. Environ. Res. Risk Assess.* **2013**, *27*, 1861–1870. [CrossRef]
26. Hao, Z.; Hao, F.; Singh, V.P.; Ouyang, W. Quantitative risk assessment of the effects of drought on extreme temperature in eastern China. *J. Geophys. Res. Atmos.* **2017**, *122*, 9050–9059. [CrossRef]
27. Lan, Y.; Shen, Y.; Zhong, Y.J.; Wu, S.F.; Wang, G.Y. Sensitivity of the mountain runoff of Urumqi River to the climate changes. *J. Arid Land Resour. Environ.* **2010**, *24*, 50–55.
28. Labat, D. Cross wavelet analyses of annual continental freshwater discharge and selected climate indices. *J. Hydrol.* **2010**, *385*, 269–278. [CrossRef]
29. Dong, L.J.; Dong, X.H.; Zeng, Q.; Wei, C.; Yu, D.; Bo, H.J.; Guo, J. Long-term runoff change trend of Yalong River basin under future climate change scenarios. *Adv. Clim. Change Res.* **2019**, *15*, 596–606.
30. Qin, P.; Xu, H.; Liu, M.; Liu, L.; Xiao, C.; Mallakpour, I.; Naeini, M.R.; Hsu, K.; Sorooshian, S. Projected impacts of climate change on major dams in the Upper Yangtze River Basin. *Clim. Change* **2022**, *170*, 8. [CrossRef]
31. Manoutsoglou, E.; Lazos, I.; Steiakakis, E.; Vafeidis, A. The Geomorphological and Geological Structure of the Samaria Gorge, Crete, Greece—Geological Models Comprehensive Review and the Link with the Geomorphological Evolution. *Appl. Sci.* **2022**, *12*, 10670. [CrossRef]
32. Lipar, M.; Ferk, M. Karst pocket valleys and their implications on Pliocene–Quaternary hydrology and climate: Examples from the Nullarbor Plain, southern Australia. *Earth-Sci. Rev.* **2015**, *150*, 1–13. [CrossRef]
33. Maity, R.; Ramadas, M.; Govindaraju, R.S. Identification of hydrologic drought triggers from hydroclimatic predictor variables. *Water Resour. Res.* **2013**, *49*, 4476–4492. [CrossRef]
34. De Sousa, L.F.; Ferraz, L.L.; Santos, C.A.S.; Rocha, F.A.; de Jesus, R.M. Assessment of hydrological trends and changes in hydroclimatic and land use parameters in a river basin in northeast Brazil. *J. S. Am. Earth Sci.* **2023**, *128*, 104464. [CrossRef]
35. Duan, K.; Yao, T.; Wang, N.; Liu, H. Numerical simulation of Urumqi Glacier No. 1 in the eastern Tianshan, central Asia from 2005 to 2070. *Chin. Sci. Bull.* **2012**, *57*, 4505–4509. [CrossRef]
36. Zhao, S.Q.; Lv, X.Y.; Wang, Z.Y.; Zhao, Z.W.; Li, Y.X. Application of Machine Learning Techniques in Agrometeorology. *Mod. Agric. Res.* **2023**, *29*, 136–139. [CrossRef]
37. Sun, J.L.; Zhang, Z.H.; Yu, W.D.; Deng, T.H. Research Progress on the Agrometeorological Automatic Observation in China. *Adv. Meteorol. Sci. Technol.* **2022**, *12*, 7–13+29. [CrossRef]
38. Zuo, G.G. Study on Mechanism and Methods of Adaptive Streamflow Forecasting Based on Machine Learning. Ph.D. Thesis, Xi’an University of Technology, Xi’an, China, 2021.
39. Wang, X.Y. Comparative Study on Agricultural Drought Monitoring in the Loess Plateau Based on Three Machine Learning Methods. Master’s Thesis, Northwest Normal University, Lanzhou, China, 2022.
40. Xu, X.J. Estimation of Reference Evapotranspiration with Machine Learning Methods under Future Climate Change. Master’s Thesis, Northwest A&F University, Yangling, China, 2022.
41. Li, X.; Zhang, L.; Zeng, S.; Tang, Z.; Liu, L.; Zhang, Q.; Tang, Z.; Hua, X. Predicting Monthly Runoff of the Upper Yangtze River Based on Multiple Machine Learning Models. *Sustainability* **2022**, *14*, 11149. [CrossRef]
42. Wang, S.; Sun, M.; Wang, G.; Yao, X.; Wang, M.; Li, J.; Duan, H.; Xie, Z.; Fan, R.; Yang, Y. Simulation and Reconstruction of Runoff in the High-Cold Mountains Area Based on Multiple Machine Learning Models. *Water* **2023**, *15*, 3222. [CrossRef]
43. Zhu, X.; Lee, S.-Y.; Wen, X.; Ji, Z.; Lin, L.; Wei, Z.; Zheng, Z.; Xu, D.; Dong, W. Extreme climate changes over three major river basins in China as seen in CMIP5 and CMIP6. *Clim. Dyn.* **2021**, *57*, 1187–1205. [CrossRef]
44. Li, X.; Zhang, K.; Gu, P.; Feng, H.; Yin, Y.; Chen, W.; Cheng, B. Changes in precipitation extremes in the Yangtze River Basin during 1960–2019 and the association with global warming, ENSO, and local effects. *Sci. Total Environ.* **2021**, *760*, 144244. [CrossRef]

45. Pang, Y.M.; Chen, C.; Xu, F.X.; Guo, X.Y. Impact of climate change on potential productivities of main grain crops in the Sichuan Basin. *Chin. J. Ecol.-Agric.* **2020**, *28*, 1661–1672. [[CrossRef](#)]
46. Li, B.Y. Impact of Climate Change and Human Activities on Hydrological Processes in Upper Reaches of the Yangtze River Basin. Ph.D. Thesis, Wuhan University, Wuhan, China, 2020.
47. National Oceanic and Atmospheric Administration, Physical Sciences Laboratory. NCEP-DOE Reanalysis 2: Summary. Available online: <https://psl.noaa.gov/data/gridded/data.ncep.reanalysis2.html> (accessed on 15 June 2023).
48. World Meteorological Organization. No. 997—Scientists Urge More Frequent Updates of 30-Year Climate Baselines to Keep Pace with Rapid Climate Change. 6 December 2015. Available online: <https://public.wmo.int/en/media/press-release/no-997-scientists-urge-more-frequent-updates-of-30-year-climate-baselines-keep> (accessed on 15 June 2023).
49. World Meteorological Organization. *WMO Guidelines on the Calculation of Climate Normals*; WMO: Geneva, Switzerland, 2017. Available online: [https://library.wmo.int/index.php?lvl=notice\\_display&id=20130#.Xznu2ChKg2x](https://library.wmo.int/index.php?lvl=notice_display&id=20130#.Xznu2ChKg2x) (accessed on 15 June 2023).
50. An, Y.K. Coupling Simulation and Uncertainty Analysis of Surface Water and Groundwater in Hun River Basin. Ph.D. Thesis, Jilin University, Changchun, China, 2019.
51. Chen, J.; Brissette, F.P.; Leconte, R. Uncertainty of downscaling method in quantifying the impact of climate change on hydrology. *J. Hydrol.* **2011**, *401*, 190–202. [[CrossRef](#)]
52. Wan, H.; Bian, J.; Zhang, H.; Li, Y. Assessment of future climate change impacts on water-heat-salt migration in unsaturated frozen soil using CoupModel. *Front. Environ. Sci. Eng.* **2020**, *15*, 10. [[CrossRef](#)]
53. Gilbert, R.O. *Statistical Methods for Environmental Pollution Monitoring*; Wiley: Hoboken, NJ, USA, 1987.
54. Wilby, R.L.; Dawson, C.W.; Barrow, E.M. sdsms—A decision support tool for the assessment of regional climate change impacts. *Environ. Model. Softw.* **2002**, *17*, 145–157. [[CrossRef](#)]
55. Wilby, R.L.; Dawson, C.W. The Statistical DownScaling Model: Insights from one decade of application. *Int. J. Climatol.* **2013**, *33*, 1707–1719. [[CrossRef](#)]
56. Hamed, K.H.; Ramachandra Rao, A. A modified Mann-Kendall trend test for autocorrelated data. *J. Hydrol.* **1998**, *204*, 182–196. [[CrossRef](#)]
57. Mann, H.B. Nonparametric test against trend. *Econometrica* **1945**, *13*, 245–259. [[CrossRef](#)]
58. Kendall, M.G. *Rank Correlation Methods*; Griffin: London, UK, 1948.
59. Xianghui, L.U.; Hua, B.; Ya, L.V.; Benjia, Z. Analysis on Historical Weather and Prediction of Future Climate Change in Jiangxi Province. *Res. Soil Water Conserv.* **2015**.
60. Yonaba, R.; Tazen, F.; Cissé, M.; Mounirou, L.A.; Belemtougri, A.; Ouedraogo, V.A.; Koïta, M.; Niang, D.; Karambiri, H.; Yacouba, H. Trends, sensitivity and estimation of daily reference evapotranspiration ET<sub>0</sub> using limited climate data: Regional focus on Burkina Faso in the West African Sahel. *Theor. Appl. Climatol.* **2023**, *153*, 947–974. [[CrossRef](#)]
61. Yue, S.; Wang, C.Y. Applicability of prewhitening to eliminate the influence of serial correlation on the Mann-Kendall test. *Water Resour. Res.* **2002**, *38*, 4-1–4-7. [[CrossRef](#)]
62. Asarian, J.E.; Walker, J.D. Long-Term Trends in Streamflow and Precipitation in Northwest California and Southwest Oregon, 1953-2012. *JAWRA J. Am. Water Resour. Assoc.* **2016**, *52*, 241–261. [[CrossRef](#)]
63. Shourov, M.M.; Mahmud, I. pyMannKendall: A python package for non parametric Mann Kendall family of trend tests. *J. Open Source Softw.* **2019**, *4*, 1556. [[CrossRef](#)]
64. Xiao, S.M.; Liu, T. Medium-term and long-term Forecast of Reservoir Runoff in Dry Season Based on Random Forest and Deep Neural Network. *Guangdong Water Resour. Hydropower* **2023**, 54–58.
65. Wang, Y.X.; Liu, X.; Shen, Y.J. Applicability of the random forest model in quantifying the attribution of runoff changes. *Chin. J. Eco-Agric.* **2022**, *30*, 864–874. [[CrossRef](#)]
66. Thompson, C.G.; Kim, R.S.; Aloe, A.M.; Becker, B.J. Extracting the Variance Inflation Factor and Other Multicollinearity Diagnostics from Typical Regression Results. *Basic Appl. Soc. Psychol.* **2017**, *39*, 81–90. [[CrossRef](#)]
67. Salmerón Gómez, R.; García Pérez, J.; López Martín, M.D.M.; García, C.G. Collinearity diagnostic applied in ridge estimation through the variance inflation factor. *J. Appl. Stat.* **2016**, *43*, 1831–1849. [[CrossRef](#)]
68. Singh, A.K.; Kumar, P.; Ali, R.; Al-Ansari, N.; Vishwakarma, D.K.; Kushwaha, K.S.; Panda, K.C.; Sagar, A.; Mirzania, E.; Elbeltagi, A.; et al. An Integrated Statistical-Machine Learning Approach for Runoff Prediction. *Sustainability* **2022**, *14*, 8209. [[CrossRef](#)]
69. Sharifi, A.; Dinpashoh, Y.; Mirabbasi, R. Daily runoff prediction using the linear and non-linear models. *Water Sci. Technol.* **2017**, *76*, 793–805. [[CrossRef](#)]
70. Xie, S.; Zhang, K.; Li, Y.; Dai, C. Establishment of Low Water Runoff Forecast Model in Yichun River Basin by Multiple Linear Regression Method. *IOP Conf. Ser. Earth Environ. Sci.* **2020**, *474*, 072067. [[CrossRef](#)]
71. Guo, C.W. Application of Combined Multiple Linear Regression Model in Runoff Prediction. *Pearl River* **2021**, *42*, 49–55. [[CrossRef](#)]
72. Li, Y.J.; Li, X.; Tian, C.S. Application of Multiple Regression Method in Dry Season Runoff Forecast of Yichun River Basin. *Water Resour. Plan. Des.* **2016**, *10*, 36–37. [[CrossRef](#)]
73. Wu, H.; Lei, H.; Lu, W.; Liu, Z. Future changes in precipitation over the upper Yangtze River basin based on bias correction spatial downscaling of models from CMIP6. *Environ. Res. Commun.* **2022**, *4*, 045002. [[CrossRef](#)]
74. Guan, Y.H. Extreme Climate Change And Its Trend Prediction in the Yangtze River Basin. Ph.D. Thesis, Northwest A&F University, Yangling, China, 2015.

75. Jiang, T.; Lv, Y.R.; Huang, J.L.; Wang, Y.J.; Su, B.D.; Tao, H. New Scenarios of CMIP6 Model (SSP-RCP) and Its Application in the Huaihe River Basin. *Adv. Meteorol. Sci. Technol.* **2020**, *10*, 102–109. [[CrossRef](#)]
76. Chen, T.; Zou, L.; Xia, J.; Liu, H.; Wang, F. Decomposing the impacts of climate change and human activities on runoff changes in the Yangtze River Basin: Insights from regional differences and spatial correlations of multiple factors. *J. Hydrol.* **2022**, *615*, 128649. [[CrossRef](#)]
77. Maraun, D. Bias Correcting Climate Change Simulations—A Critical Review. *Curr. Clim. Change Rep.* **2016**, *2*, 211–220. [[CrossRef](#)]
78. Yonaba, R.; Biaou, A.C.; Koïta, M.; Tazen, F.; Mounirou, L.A.; Zouré, C.O.; Queloz, P.; Karambiri, H.; Yacouba, H. A dynamic land use/land cover input helps in picturing the Sahelian paradox: Assessing variability and attribution of changes in surface runoff in a Sahelian watershed. *Sci. Total Environ.* **2021**, *757*, 143792. [[CrossRef](#)]

**Disclaimer/Publisher’s Note:** The statements, opinions and data contained in all publications are solely those of the individual author(s) and contributor(s) and not of MDPI and/or the editor(s). MDPI and/or the editor(s) disclaim responsibility for any injury to people or property resulting from any ideas, methods, instructions or products referred to in the content.